T.C. DOKUZ EYLÜL
UNIVERSITY IZMIR
INTERNATIONAL
BIOMEDICINE AND GENOME
INSTITUTE

# A Modular Scan Head for Optical Coherence Tomography Guided Laser Nerve Stimulation

Hanife GÖKKAN

DEPARTMENT OF BIOMEDICINE AND HEALTH TECHNOLOGIES

**MASTER OF SCIENCE THESIS**

**İZMİR-2024**

**TEZ KODU: DEU.IBG.MSc/2020850031**

T.C. DOKUZ EYLÜL UNIVERSITY IZMIR
INTERNATIONAL BIOMEDICINE AND GENOME
INSTITUTE

# A Modular Scan Head for Optical Coherence Tomography Guided Laser Nerve Stimulation

DEPARTMENT OF BIOMEDICINE AND HEALTH TECHNOLOGIES

**MASTER OF SCIENCE THESIS**

**Hanife GÖKKAN**

Supervisor: Assoc. Prof. Dr. Serhat TOZBURUN

(This research is supported by TÜBİTAK grant No:121E375)

**TEZ KODU:** DEU.IBG.MSc/PhD-Student number

T.C.
DOKUZ EYLÜL ÜNİVERSİTESİ
İZMİR ULUSLARARASI BİYOTIP VE GENOM ENSTİTÜSÜ

# YÜKSEK LİSANS TEZ SAVUNMA SINAVI TUTANAĞI

Dokuz Eylül Üniversitesi İzmir Uluslararası Biyotıp ve Genom Enstitüsü Biyotıp ve Sağlık Teknolojileri Anabilim Dalı Biyotıp ve Sağlık Teknolojileri Yüksek Lisans Programı 2020850031 numaralı öğrencisi Hanife Gökkan, "**A Modular Scan Head for Optical Coherence Tomography Guided Laser Nerve Stimulation**" konulu Yüksek Lisans tezini 12.02.2024 tarihinde yapılan savunma sınavı sonucunda başarılı olmuştur.

**BAŞKAN**

Doç. Dr. Serhat TOZBURUN
Dokuz Eylül Üniversitesi

**JÜRİ ÜYESİ**

Doç. Dr. Sinan GÜVEN
Dokuz Eylül Üniversitesi

**JÜRİ ÜYESİ**

Doç. Dr. Hüseyin Cumhur TEKİN
İzmir Yüksek Teknoloji Enstitüsü

# TABLE OF CONTENTS


TABLE OF CONTENTS i
LIST OF TABLES ii
LIST OF FIGURES iii
LIST OF ABBREVIATIONS vi
ACKNOWLEDGEMENTS viii
ABSTRACT 1
Özet 3
1.INTRODUCTION AND AIM 5
1.1.Statement and Importance of the Problem 5
1.2. Aim of the Study 5
2.GENERAL INFORMATION 7
2.1. Vagus Nerve Stimulation 7
2.2. Challenges in Laser Nerve Stimulation 9
2.3 Optical Coherence Tomography (OCT) 10
3.MATERIALS AND METHODS 12
3.1. Type of the Study 12
3.2. Time and Location of the Study 12
3.3. The Universe and Sample of Research 12
3.4. Working Materials 12
3.5. Variables of Study 12
3.6. Data Collection Tools 13
3.6.1. Stretched-pulse Mode-locked (SPML) Wavelength-swept Laser 13
3.6.2. Timing Jitter Analysis 14
3.6.3 Interferometer Setup 15
3.6.4 1500 nm Laser Nerve Stimulation 16
3.6.5 Construction of the Custom-designed Modular Scanning Head 18
3.6.6 Beam Waist Measurements Using Knife-edge Method 20
3.6.7 Characterization of the Surface Scanning Performance 22
3.6.8 Integrating Laser Beams, CMOS and Thermal Cameras 23
3.6.9 Preparation of An Agar Phantom 24
3.7. Research Plan 25
3.8. Data Evaluation 27
3.9. Limitations of the Study 27
3.10. Ethics Approval 27
4. RESULTS 28
4.1 Lasing Performance of the SPML Laser 28

4.2 Timing Jitter 30
4.3 OCT Performance of the SPML Laser 31
4.4 Performance of the Custom-designed Modular Scanning Head at 1505 nm Used for LNS 33
4.5 Beam Waist Measurements 35
4.6 Laser Energy Analysis of 1505 nm Laser for Continuous Wave Mode and Modulated Mode 36
4.7 Integrating Thermal and Digital Cameras 39
4.8 Phantom Trials of the Integrated System 40
5. DISCUSSION 43
6. CONCLUSION AND FUTURE DIRECTIONS 45
7.References 47
8. APPENDIX 52

**LIST OF TABLES**

**Table 1.** Ingredients and quantities used in a 100 ml agar-based phantom. 24

**LIST OF FIGURES**

**Figure 1** Illustration of a hook electrode and electrical current to initiate action potential in the nerve bundle [14]. 8

**Figure 2.** Simple block diagram of OCT setup 10

**Figure 3.** Schematic of the stretched-pulse mode-locked laser. SOA: semiconductor14

**Figure 4.** Schematic of the timing jitter measurement setup. 15

**Figure 5.** Schematic of the balanced Mach-Zehnder interferometer. BD: Balanced photodetector (1.6 GHz). PD: Photodetector (25 GHz). CL: collimator (f = 18.67 mm). DC: Dispersion compensator. M: Mirror. OSC: Oscilloscope (~40 GS/s); OSA: Optical Spectrum Analyzer (AQ6370D, Yokogawa). 16

**Figure 6.** A 500 mW, single-mode fiber-coupled diode laser that produces a laser beam at a wavelength of 1505 nm. The diode laser is driven with three drivers. 17

**Figure 7.** The probe operating at 1284-nm center wavelength for OCT, 1505 nm wavelength laser for LNS and CMOS for visible wavelength.The function generator is directly connected to the optical oscillator driver of the 1.505 μm wavelength laser for LNS. Lasers can be operated in continuous waveform or pulse form driven by square wave electrical signals. 17

**Figure 8. (A)** Beam optics simulation results of the probe design. **(B)** Custom-designed microscope. **(C)** Optical insertion loss was estimated at ~12% in the visible and ~35% in the near-infrared range. 19

**Figure 9.** Block diagram of the laser power measurement setup. NDF: Neutral density filter. D: Sensor. 20

**Figure 10.** Schematic of the knife edge measurement technique to measure the beam waist focused by the probe. D: Sensor. J: Sharp-edged razor. 21

**Figure 11.** Diagram of the knife-edge measurement technique for measuring the waist of light scanned by the Galvo Mirror. 21

**Figure 12. (A)** The mechanism in which the scanning mirror is calibrated. **(B)** Specially designed mirror holder. **(C)** Scanning distances at 1 kHz can be adjusted depending on the amplitude of the electrical signal. 22

**Figure 13.** Photograph of the final version of the modular scanning head and externally included thermal camera. 23

**Figure 14.** Variation of narrow electrical pulses produced by the optical amplitude

modulator concerning the clock signal pulse. The narrowest linewidth was 212.8 ps.29
**Figure 15.** Average measurement results and standard deviation of the bias voltage applied to the amplitude modulator in each clock signal bandwidth condition. N=3.29
**Figure 16.** Representative spectral output of the SPML laser. The measured optical bandwidth is 105 nm at a center wavelength of 1283.72 nm. 30
**Figure 17.** Tentative time-domain output of the SPML laser. Repetition rate of the optical pulses is 22.70417 MHz at 88% duty cycle. 30
**Figure 18.** Electrical signal examples produced by the function generator are plotted on each other. The jitter/standard deviation value was measured at approximately ~3-μs at the time the generator had. 31
**Figure 19.** Tentative fringe signals recorded for the optical path length difference between 0.1 mm and 1.2 mm at a step size of 0.01 mm. OPD: Optical path length difference. 32
**Figure 20.** Estimated corresponding point spread functions The axial resolution was 18.1 μm in the air and the SPML laser produced a coherence length of 0.6 mm in the single-pass configuration. 33
**Figure 21.** Absorption coefficient (blue line) and optical penetration depth (red line) in water along the near-infrared optical wavelength [12]. The dashed black line indicates the laser wavelength used in the study, which provides optical penetration depth that closely matches the diameters of peripheral nerves in rats. 34
**Figure 22.** Variation of laser power according to the electric current applied to the chip of the diode laser. **(A)** Due to the limited optical damage threshold of the sensor in laboratory measurement, the electric current was scanned with a range of 100 mA increments up to a value of 2 A. **(B)** Measurement chart provided by the manufacturer. The pink line indicates the change in the potential difference (voltage) applied to the chip of the diode laser according to the electric current. 35
**Figure 23.** Results of beam diameter measurements. The beam diameter at position 1 (0 Volt) was 18.6 μm for 1284 nm (A) and 22.1 μm for 1505 nm (B). The beam diameter at position 2 (0.5 Volt) was 20.2 μm for 1284 nm (C) and 20.4 μm for 1505 nm (D). The beam diameter at position 3 (1.3 Volt) was 20.4 μm for 1284 nm (E) and 19.5 μm for 1505 nm (F). 36
**Figure 24**. Examples of square wave signals the function generator produces at different duty cycles (10%, 25%, 50%, 75%, 90%). **(A)** 10 Hz repetition rate. **(B)** 20 Hz repetition rate. **(C)** 30 Hz repetition rate. **(D)** 40 Hz repetition rate. **(E)** 50 Hz repetition rate. **(F)**

100 Hz repetition rate. **(H)** 150 Hz repetition rate. **(G)** 200 Hz repetition rate. 38
**Figure 25.** Determined laser energy for different repetition rates and duty cycles. The laser energy produced in the continuous wave case is also placed in the graph with an orange column for direct comparison. 39
**Figure 26. (A)** Image of an IR card captured with a CMOS camera during 1284 nm laser irradiation. **(B)** Image of an IR card captured with a CMOS camera during 1505 nm laser irradiation. **(C)** Representative superimposed image. 40
**Figure 27. (A)** An example of a produced fringe signal (i.e., OCT signal) from a single point on the sample. **(B)** Real-time imaging using a CMOS camera in the visible range at 30 fps. **(C)** Tentative thermal camera view of the sample during laser irradiation. 41
**Figure 28.** Depth-resolved amplitude changes of fringe signals (OCT signals) before, during, and after 1500 nm laser exposure. Thermal camera measured the surface temperature as 22°C, 45°C, and 22°C, respectively. 42

**LIST OF ABBREVIATIONS**

LNS: laser nerve stimulation
ENS: Electrical Nerve Stimulation
OCT: Optical Coherence Tomography
PNS: Peripheral Nerve Stimulation
TENS: Transcutaneous electrical nerve stimulation
VNS: Vagus Nerve Stimulation
SPML: Stretched-Pulse Mode-Locked
OPD: Optical path length difference.
CL: Bi-Convex Lens
SL: Scan Lens
CMOS: Camera
DM:Dichroic Mirror
AL:Achromatic Lens
GM: Galvo Mirror
mm: millimeter
nm: nanometer
μm: micrometer
mW: milliwatt
Hz: Hertz
GHz: Gigahertz
MHz: Megahertz
kHz: kilohertz
S: Second
Ns: Nanosecond
Ps: Picosecond
dB: Decibel
BD: Balanced photodetector
PD: Photodetector
DC: Dispersion compensator
M: Mirror
OSC: Oscilloscope
OSA: Optical Spectrum Analyzer
D: Sensor. J: Sharp-edged razor

ml: Milliliter

g: Gram

A: Ampere

mA: milliampere

DC: Direct Current

Fps: Frame Rate

## ACKNOWLEDGEMENTS

First and foremost, I am pleased to express my gratitude to my advisor, Serhat Tozburun, for his constant help and excellent supervision over the last three years. We have overcome all the difficulties and impossibilities together in this study. I appreciate his wife and family's acceptance and patience during the research and thesis preparation process.

This work is supported by the Scientific and Technological Research Institution of Türkiye (TUBITAK) grand no 121E375.

I am very grateful to İbrahim Akkaya for all the helpful advice. Completion of this project would not have been possible without the support of former and current T-Lab members. I want to thank Merve Türker Burhan and Güldeniz Gülcan for their valuable friendship and Seval Ünal, Berfin Arlı, and Müge Topçu for constantly motivating me and having fun. I want to thank Emre Güralp for our sleepless nights and help during the project delivery phase.

I want to thank all my friends and cousins, especially Şevin Ay and Hülya Şahin, who make my life livelier. Thanks so much to Resul Özbilgiç for always being there for me and motivating me. It was a challenging time, but you made it more accessible.

I want to thank my sister, Betül Gökkan, for his endless help and encouragement. I couldn't have done this without his support. I hope this thesis will be an inspiration to my nephew Ahmet Aren Gökkan and Betül Gökkan, who just started their life journey. I know that they will be better than me. I want to express my heartfelt gratitude to my brother Ali Osman Gökkan and his wife Esin Gökkan for their presence, love, and tolerance. Their belief in me has kept my spirits and motivation high during this process.

Finally, I am eternally grateful to my parents, Rahime Gökkan and Ahmet Gökkan, for their support, patience, and love from the beginning of my life. I wish to dedicate this thesis to my parents.

A Modular Scan Head for Optical Coherence Tomography Guided Laser Nerve Stimulation

**Hanife GÖKKAN, İzmir International Biomedicine and Genome Institute, Dokuz Eylul University Health Campus, Balcova 35340 - Izmir / TURKEY**

## ABSTRACT

The laser nerve stimulation (LNS) technique has several advantages over the traditional electrical nerve stimulation (ENS) technique: (1) Non-invasive nerve stimulation method; (2) Enhanced spatial selectivity; (3) Elimination of measurement errors caused by electrical interference in measurements. However, one issue that limits these advantages is that the tissue temperature for a successful and safe LNS is restricted to a narrow window (41 °C – 48 °C). Another limitation is that a conventional thermal camera can measure only instantaneous surface temperature. For these reasons, to successfully transfer the LNS technique to clinical applications, especially nerve stimulation applications in critical areas, a control approach is needed to monitor the depth-resolved temperature change in the nerve. Optical Coherence Tomography (OCT), an emerging 3D imaging method, may be a candidate for monitoring laser-induced temperature increase from the surface and depth of neural tissue.

This thesis studies a custom-designed modular scanning head (i.e., optical probe) design for OCT-guided laser nerve stimulation. The design aligns and focuses the 1505 nm laser beam for LNS and the 1284 nm laser beam for OCT. It also includes a metal oxide semiconductor camera for complementary real-time imaging of the nerve surface in a visible optical range. The custom-designed OCT system uses a stretched-pulse mode-locked laser source that provides a sweep rate of 22.7 MHz over a 105 nm range at a center wavelength of 1284nm. By providing the OCT signal in M mode, the change in fringe amplitude as a function of laser-induced temperature change between 41 °C – 48 °C was successfully measured in a phantom model. The developed optical probe can be used in OCT-guided LNS studies in a preclinical animal model by adding a phase-locked 2D scanner.

**Keywords:** Laser nerve stimulation, swept-source optical coherence tomography, optical probe, M-mode imaging.

A Modular Scan Head for Optical Coherence Tomography Guided Laser Nerve Stimulation

**Hanife GÖKKAN, İzmir Uluslararası Biyotıp ve Genom Enstitüsü, Dokuz Eylül Üniversitesi**
**Sağlık Yerleşkesi, Balçova 35340- İzmir / TÜRKİYE**

## Özet

Lazer sinir stimülasyonu (LNS) tekniğinin, geleneksel elektriksel sinir stimülasyonu (ENS) tekniğine göre çeşitli avantajları vardır: (1) Non-invaziv sinir stimülasyon yöntemi; (2) Geliştirilmiş mekânsal seçicilik; (3) Ölçümlerdeki elektriksel girişimden kaynaklanan ölçüm hatalarının ortadan kaldırılması. Ancak bu avantajları sınırlayan bir konu, başarılı ve güvenli bir LNS için doku sıcaklığının dar bir pencereyle (41 °C – 48 °C) sınırlı olmasıdır. Diğer bir sınırlama ise geleneksel bir termal kameranın yalnızca anlık yüzey sıcaklığını ölçülebilmesidir. Bu nedenlerden dolayı, LNS tekniğinin klinik uygulamalara, özellikle de kritik bölgelerdeki sinir stimülasyon uygulamalarına başarılı bir şekilde aktarılabilmesi için, sinirdeki derinlik çözümlü sıcaklık değişiminin izlenmesini sağlayacak bir kontrol yaklaşımına ihtiyaç vardır. Yeni ortaya çıkan bir 3 boyutlu görüntüleme yöntemi olan Optik Koherens Tomografi (OCT), sinir dokusunun yüzeyinden ve derinliğinden lazer kaynaklı sıcaklık artışının izlenmesi için aday olabilir.

Bu tez, OCT kılavuzluğunda lazer sinir stimülasyonu için optik bir prob tasarımını incelemektedir. Tasarım, LNS için 1505 nm lazer ışınını ve OCT için 1284 nm lazer ışınını hizalar ve odaklar. Ayrıca sinir yüzeyinin görünür bir optik aralıkta tamamlayıcı gerçek zamanlı görüntülenmesi için metal oksit yarı iletken bir kamera içerir. Özel olarak tasarlanmış OCT sistemi, 1284 nm merkez dalga boyunda 105 nm aralığında 22,7 MHz tarama hızı sağlayan uzatılmış darbe modu kilitli bir lazer kaynağı kullanır. M modunda OCT sinyalinin sağlanmasıyla, 41°C ile 48°C arasında lazer kaynaklı sıcaklık değişiminin bir fonksiyonu olarak saçak genliğindeki değişiklik, bir fantom modelinde başarıyla ölçüldü. Geliştirilen prob, faz kilitli 2 boyutlu tarayıcı eklenerek klinik öncesi hayvan modelinde OCT rehberliğinde LNS çalışmalarında kullanılabilir.

**Anahtar kelimeler:** Lazer sinir stimülasyonu, taranmış kaynaklı optik koherens tomografi, optik prob, M-mod görüntüleme.

# 1.INTRODUCTION AND AIM

## 1.1.Statement and Importance of the Problem

Using near-infrared laser energy, laser nerve stimulation (LNS) represents a non-invasive method that offers several advantages over electrical nerve stimulation (ENS). It provides improved spatial selectivity and eliminates electrical artifacts in measurements. However, the success of LNS is hindered by the strict temperature range (41 °C – 48 °C) required for safe and reliable nerve stimulation and the limitation of conventional thermal cameras that can only measure instantaneous surface temperatures. These challenges hinder the smooth transition of LNS into clinical settings, particularly in nerve stimulation. An approach that measures depth-resolved temperature changes within neural tissue could address these limitations. OCT is emerging as a 3D imaging modality to monitor laser-induced temperature changes at the surface and within the nerve bundle during LNS.

The thesis explores the design of an optical probe tailored for OCT-guided laser nerve stimulation. The probe aligns and focuses the LNS and OCT laser beams and employs a metal oxide semiconductor camera for real-time visible imaging. The proposed probe design is promising for advancing the LNS technique, offering a pathway for safe, reliable, and repeatable nerve stimulation, especially in preclinical animal studies.

## 1.2. Aim of the Study

The study aims to create and characterize a scanning head (optical probe) that focuses on a 1505 nm laser beam for laser nerve stimulation, a 1284 nm laser beam for Optical Coherence Tomography, and a camera for surface imaging in the visible range. The study combines four substudies: (i) building a custom-design Optical Coherence Tomography system using a stretched-pulse mode-locked laser (ii) simulation based on ray optics, (iii) design, construction, and characterization of the benchtop scanning head, and (iv) testing through a phantom model.

### 1.3. Hypothesis of the Study

A narrow temperature range (41 °C – 48 °C) for successful, reliable, and safe nerve stimulation remains challenging for laser nerve stimulation, an emerging stimulation method. Optical Coherence Tomography (OCT) may offer a solution for monitoring thermal change within the nerve bundle by providing real-time, depth-resolved temperature assessments during laser irradiation. The study hypothesizes that a designed optical probe can be used for OCT-guided laser nerve stimulation.

## 2.GENERAL INFORMATION

### 2.1. Vagus Nerve Stimulation

Stimulation of the peripheral nerve is traditionally used to relieve pain in different peripheral nerves. Electrical nerve stimulation (ENS) is emerging as a pioneer and heralding a paradigm shift towards non-invasive stimulation applications [1]. Although ENS approaches are widely used in pain management, recent studies suggest that various peripheral nerve stimulation (PNS) techniques should be compared for better clinical outcomes [2]. An acceptable assessment of the contemporary nerve stimulation milieu reveals the centrality of Transcutaneous electrical nerve stimulation (TENS) in pain control, accentuating its multifaceted efficacy [3]. ENS includes applications in various fields ranging from disorders such as urinary incontinence [4]. Continues to modern neurostimulation paradigms, where a transformational landmark is the groundbreaking effect of deep brain stimulation in reducing Parkinson's disease symptoms [5]. The development of vagus nerve stimulation (VNS), revealing historical perspectives, addresses the critical issue, and empirical research highlights its tremendous effectiveness in managing seizures and other neurological applications [6–9]. Within this historical continuum, the focus narrows to explain the noteworthy effect of VNS on the landscape of neurological disorders. VNS emerges as a transformative therapeutic modality, with practical examinations confirming its pivotal role in reducing seizure activity via trigeminal and VNS [8–10]. A penetrating investigation into the speeds and determinants of seizure release highlights the inherent promise encapsulated within VNS [11,12]. Prospective long-term research sheds light on the enduring significance of VNS in refractory seizures, propelling its integration into mainstream strategies for the treatment of epilepsy [13]. The therapeutic ambit of VNS experiences broad diversification, encompassing applications in depression treatment and the synchronization of VNS with BOLD fMRI signals [14–16]. As the therapeutic horizons burgeon, VNS adopts new paradigms that demonstrate its effectiveness in different clinical conditions and highlight its potential in selective vagus nerve stimulation [17–19]. Figure 1 shows an illustration of the VNS device surgically attached to the VN.

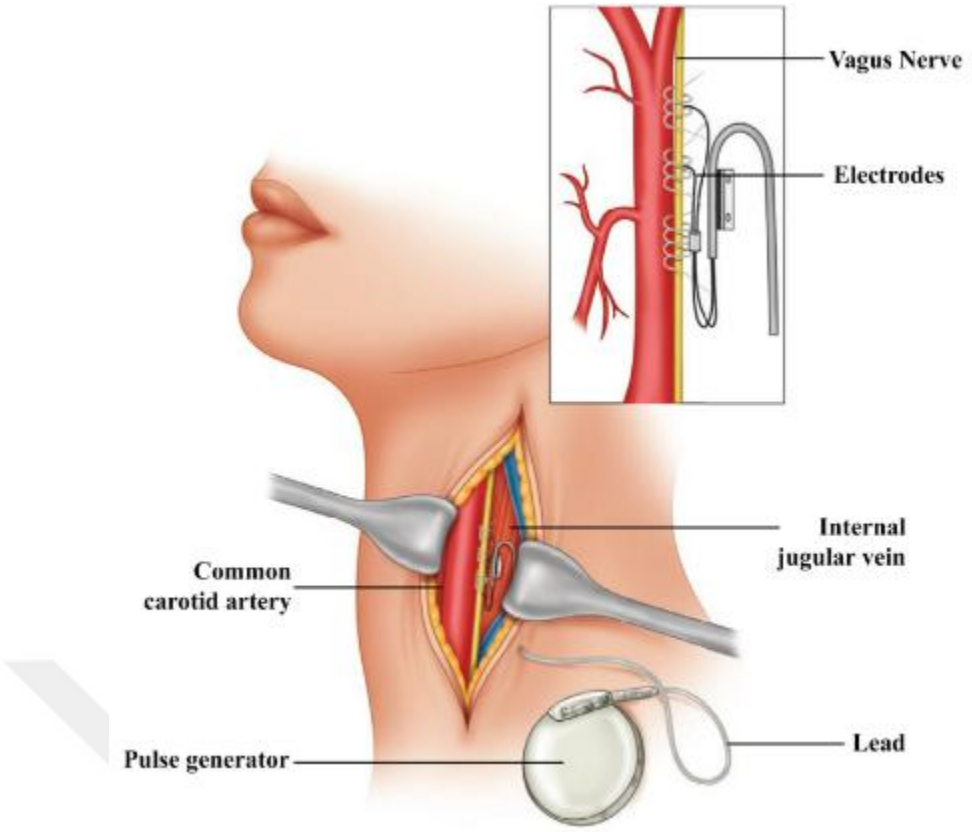



**Figure 1** Illustration of a hook electrode and electrical current to initiate action potential in the nerve bundle [14].

The narrative concludes with an insight into the future of neuromodulation, characterized by the emergence of laser nerve stimulation using near-infrared laser energy and its transformative potential in reshaping the boundaries of non-invasive neuromodulation. Recent scientific studies point to a new era marked by the laser stimulation of neural tissue in vivo, leading to a paradigmatic shift towards non-invasive neuromodulation methods [20]. Investigation of temporal dynamics and underlying biophysical mechanisms during infrared neural stimulation promises to uncover hitherto unexplored regions in precise neuromodulation [21,22]. From the mediation of infrared laser-evoked responses via TRPV4 channels to the modulation of cellular capacitance through infrared light, the symbiosis of optics and neuroscience offers unique insights into the complex interplay underlying neuromodulation with laser energy [23–25].

## 2.2. Challenges in Laser Nerve Stimulation

Laser nerve stimulation using near-infrared laser radiation has been introduced as a potential alternative to electrical techniques [26]. This new stimulation technique provides several benefits, including contactless delivery of an external stimulus, improved spatial selectivity, and elimination of stimulation artifacts [27]. The potential of LNS, a non-contact (i.e., mm-scale distance) neuromodulation technique, holds great promise for clinical applications.

The working principle of laser stimulation of peripheral nerves is still a controversial issue. The generally accepted idea is that some ion channels (e.g., TRPV4) are triggered above a certain temperature threshold by converting laser energy into heat energy [28]. However, translation of the laser-based simulation technique into general clinical use still requires rigorous parameter optimization through animal and clinical studies.

The thermal dynamics of nerve tissue during laser irradiation play a crucial role in the fragile balance between successful nerve stimulation and the release of thermal damage under certain temperature limitations. In addition to ensuring successful nerve stimulation, it may also be necessary to eliminate the potential for thermal damage, which requires precision in temperature control. Therefore, safe, reliable, and reproducible LNS depends on meticulous regulation of tissue temperature during laser irradiation within a therapeutic window of 41 – 48 °C [29-30].

Maintaining the nerve tissue temperature within a narrow range of temperatures during laser irradiation is a critical challenge for safe, reliable, and reproducible LNS. For example, controlling the rise in temperature during laser irradiation poses a challenge. Besides, going beyond this carefully defined therapeutic window carries the risk of driving the LNS to be useless, on the other hand, causing local but potentially harmful laser-induced thermal damage to the nerve bundle [31]. Thus, the inherent risks associated with failed nerve stimulation and the possibility of thermal damage highlight the limitation of the emerging simulation technique.

In addition to the narrow therapeutic thermal window, surface temperature measurements do not provide sufficient information to understand the complex thermal dynamics within the delicate nerve bundle. Given the laser's residual thermal effect on the subsurface, measuring surface temperature alone may not be sufficient to protect the delicate nerve from thermal damage. Recent studies for temperature assessment during LNS are mainly based on instantaneous surface temperature measurement [32]. However,

the superficial temperature measurement has limitations, particularly the ability to provide complete information about thermal dynamics within tissue [33]. Thus, depth-resolved thermal analysis of the nerve tissue can prevent unintentional residual thermal damage. Bringing together the requirements for translating VNS to clinical settings and recent advances in LNS, a system that analyzes the depth-resolved thermal change may contribute significantly to the ongoing report on advancing neuromodulation technologies.

### 2.3 Optical Coherence Tomography (OCT)

Optical Coherence Tomography is divided into two main branches: time-domain OCT and Fourier-domain OCT. The recently developed Fourier domain OCT model provides faster (MHz) imaging with significantly higher imaging sensitivity [34,35]. Thus, it advances the OCT technique and may become a point of attraction in medical imaging as a diagnostic tool. The Fourier-domain OCT model is further divided into two; Spectral-domain OCT and swept-source OCT, respectively. A swept-source OCT device consists of four essential parts (Figure 2): A laser source that can rapidly sweep a wide optical band range, an interferometer, an imaging probe (i.e., optical probe in this study), and data acquisition and processing.

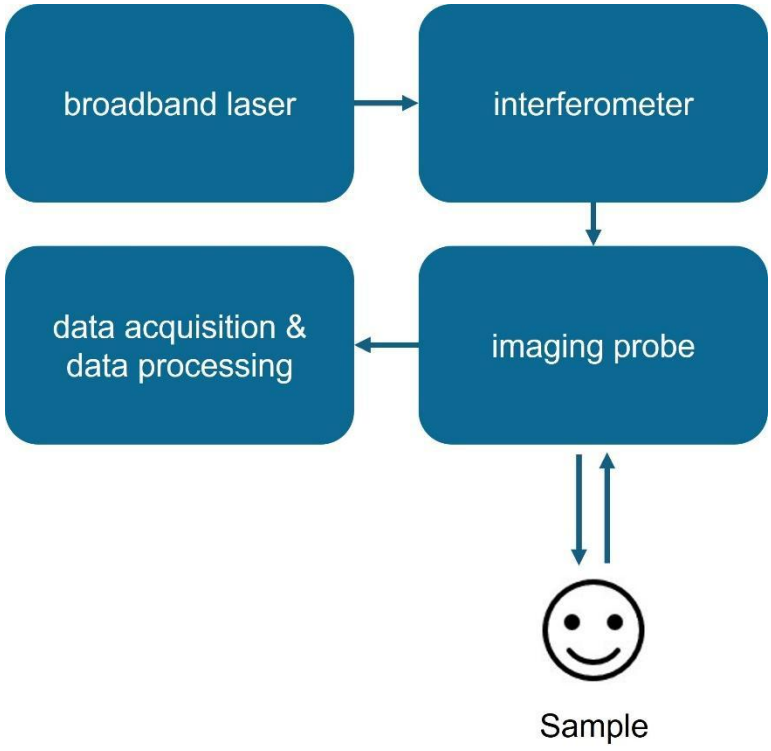



**Figure 2.** Simple block diagram of OCT setup

The laser source determines critical parameters of the swept-source OCT, such as axial resolution, A-line rate, coherence length, and measurable sensitivity level. The interferometer creates interference patterns by amplifying the first scattered photons from the sample with photons reflected from the reference mirror. Each interference pattern provides information about the biological tissue as a function of depth. The imaging probe focuses A-line scans to the sample surface, collects the photons that make the first scatter from the sample, and transmits them to the interferometer. The optical interference pattern is first converted into an analog signal by a fast optical detector (>GHz) and then converted into a digital signal by the data acquisition and processing module. The computer and particular computing model transform the digital signal into grayscale images.

OCT is a revolutionary imaging technology with profound essences for three-dimensional imaging with high optical resolution [36,37]. Considering the benefits of OCT, it stands out as an optical imaging model that pioneers applications to prevent thermal damage. Central to the success of OCT are detailed imaging principles that distinguish it from established methods. Ensuring high-resolution imaging of biological tissues is important for the development of technologies and methodologies in pre-clinic and clinical studies. By leveraging the coherence of light, OCT achieves the extraordinary depth-resolving imaging required for subtle assessments of tissue systems [35]. The diagnostic capabilities of OCT are based on the examination of backscattered light and provide valuable information about tissue structural changes. The diagnostic capabilities, which offer a non-invasive tool to assess thermal changes within the tissue, can become particularly important in LNS [38]. OCT's depth-resolved thermal imaging capability can pave the way for real-time monitoring and tailored temperature control during laser nerve interactions [39].

On the other hand, proper integration of OCT into the LNS requires precise alignment of the LNS laser beam and the OCT beam. This complex coordination enables synchronized imaging and monitoring, providing the basis for improved precision in thermal damage control. Interferometric signals during LNS can contribute to answering fundamental research questions such as deciphering the mechanisms of neuromodulator environmental signals such as temperature rise.

# 3.MATERIALS AND METHODS

## 3.1. Type of the Study

Creation of a prototype of the Modular Scanning Head for Optical Coherence Tomography Guided Laser Nerve Stimulation

## 3.2. Time and Location of the Study

The development of a modular scan head for OCT-guided laser nerve stimulation and the optimization of optical parameters studies were completed between March 2021 and March 2024 at the Izmir Biomedicine and Genome Center Tozburun Laboratory.

## 3.3. The Universe and Sample of Research

No human specimens were used in this study.

## 3.4. Working Materials

No materials were used in this study.

## 3.5. Variables of Study

## 3.6. Data Collection Tools

### *3.6.1. Stretched-pulse Mode-locked (SPML) Wavelength-swept Laser*

Figure 3 depicts a detailed schematic of the original stretched-pulse mode-locked (SPML) wavelength-swept laser source. The ring cavity utilizes a semiconductor optical amplifier (BOA1130P, Thorlabs, USA), providing a center wavelength of 1284 nm as the gain component. To provide optical pulses, a lithium-niobate electro-optic modulator is driven by a bit pattern generator (PAT 5000, Sympuls, Germany). The pattern generator provides short electrical pulses synchronized with the harmonic of the cavity round-trip time for the mode-locking mode. A low-jitter RF signal generator (SG386, Stanford Research System, USA) externally clocks the pattern generator. The modulator has an extinction ratio of 35 dB and causes an optical insertion loss of 4.9 dB at maximum transmission.

Custom-designed continuously chirped fiber Bragg gratings (Proximion Fiber Systems, Sweden) generates highly matched 454 ps/nm and negative -454 ps/nm chromatic dispersion. The optical pulses are stretched and compressed within the ring cavity through the gratings for passive wavelength sweeping. A bias controller is locked to the modulator to compensate for any drift and maintain a high optical pulse contrast value and stability.

An optical isolator allows unidirectional oscillation and a 25% fused fiber coupler delivers the laser output. Additionally, three-pedal polarization controllers are used within the laser cavity because critical components (e.g., gratings, SAO, modulator) have some degree of polarization sensitivity.

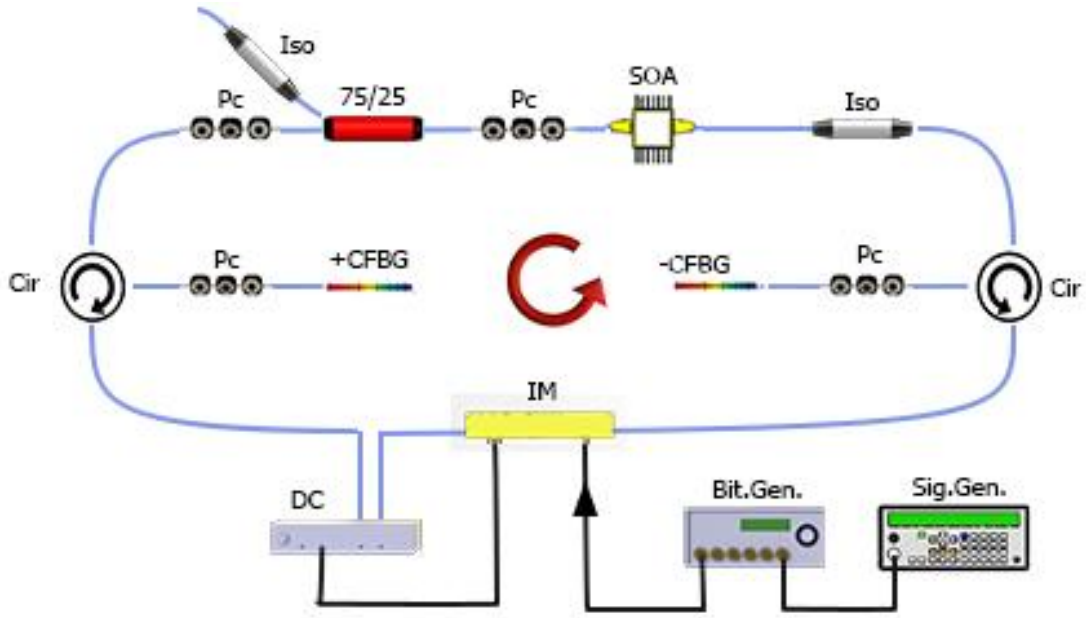



**Figure 3.** Schematic of the stretched-pulse mode-locked laser. SOA: semiconductor optical amplifier; CFBG: Chirped fiber Bragg grating Circ: Circulator; IM: Intensity modulator; ISO: isolator; PC: polarization controlling pedal; DC: bias controller.

### *3.6.2. Timing Jitter Analysis*

The timing accuracy of the electrical pulses driving the electro-optic modulator is critical to the successful operation of the SPML laser. The electrical pulse must have a jitter significantly less than the pulse width (<0.25 ns) to enable multiple optical pulses to oscillate during the optical modulator's open window. Figure 4 shows a schematic of the timing jitter measurement setup.

The measurement is carried out in several steps. 1) RF signal generators are physically phase-locked to each other. 2) The phase-locked number 1 RF generator clocks the bit generator. The phase-locked number 2 RF generator provides the oscilloscope's trigger and observation signals. 3) The frequency of the trigger signal is set higher than the frequency of the clock control signal; the trigger signal and the clock signal overlap, which is observed on the oscilloscope. 4) Phase locking between the RF signal generators is removed, and the timing jitter is measured by comparing the observation and pulse signals through an oscilloscope.

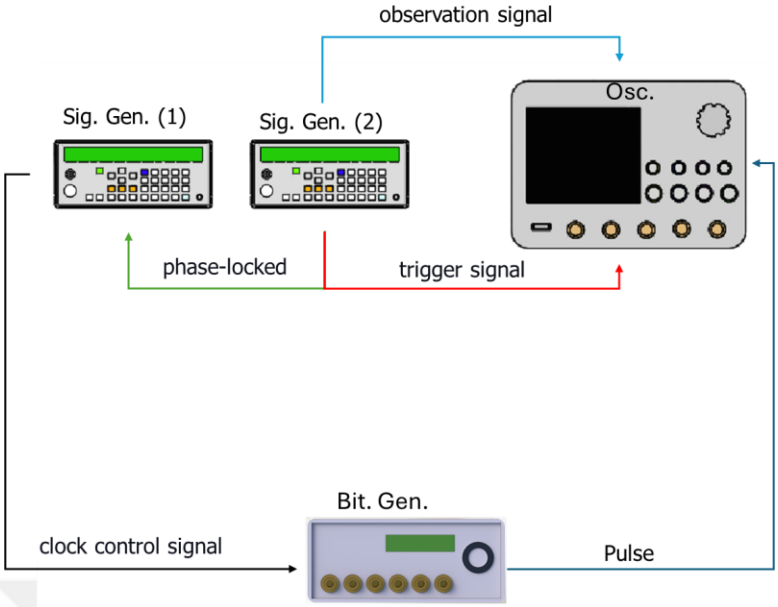



**Figure 4.** Schematic of the timing jitter measurement setup.

### *3.6.3 Interferometer Setup*

As shown in Figure 5, a fiber-based Mach-Zehnder interferometer was set to generate fringe signals. The interferometer comprises two fiber couplers at a 50/50 ratio and two optical circulators. The wavelength-swept laser beam is split into two, one into the sample arm and the other into the reference arm. The sample and reference arm circulators then collect the backscattered light, and the coupler recombines them to a 1.6-GHz balanced photodetector (PDB480C-AC, Thorlabs, USA) in two equal proportions. The photodetector detects the fringe signals produced by the interferometer. A 1.7 GHz low-pass filter (BLP1700+, Mini-circuits, USA) removes high-frequency components.

The 3.5-GHz bandwidth oscilloscope digitizes fringe signals at 40 GS/s sampling frequency as a function of the interferometer delay and stores digitized signals in onboard memory (125M points). Signals were acquired for up to a millisecond range. An optical spectrum analyzer (AQ6370D, Yokogawa, Japan) measures the laser source's power distribution over the lasing bandwidth (from 1284 nm to 1505 nm). The custom-designed modular scanning head (i.e., optical probe) on the sample arm is detailed in the following headings.

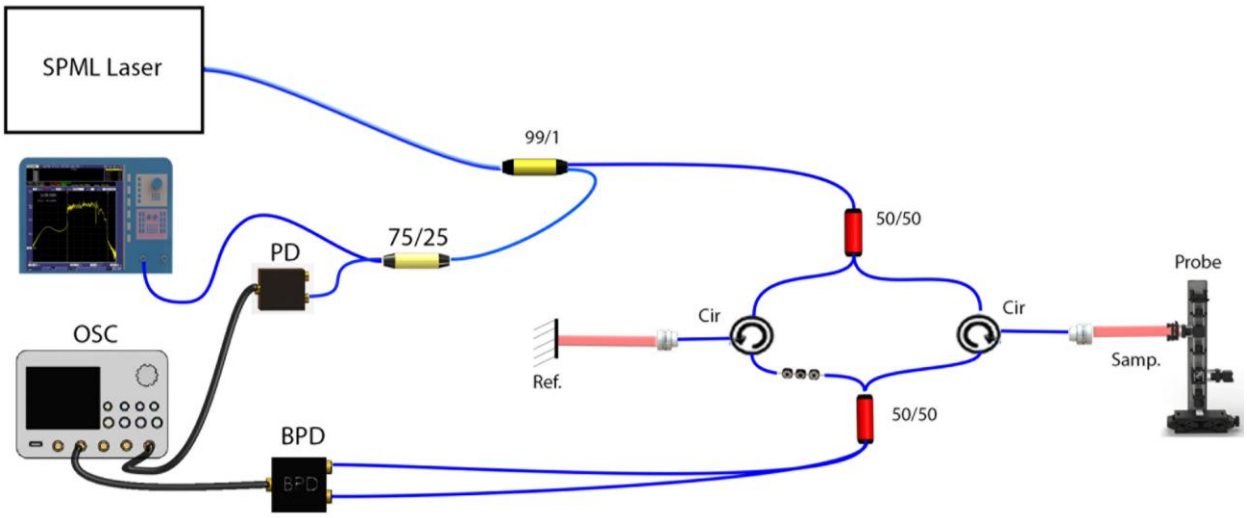



**Figure 5.** Schematic of the balanced Mach-Zehnder interferometer. BD: Balanced photodetector (1.6 GHz). PD: Photodetector (25 GHz). CL: collimator (f = 18.67 mm). DC: Dispersion compensator. M: Mirror. OSC: Oscilloscope (~40 GS/s); OSA: Optical Spectrum Analyzer (AQ6370D, Yokogawa).

### *3.6.4 1500 nm Laser Nerve Stimulation*

In laser nerve stimulation (LNS), laser energy is absorbed by the target nerve bundle, converted into heat energy, and opened ion channels, such as TRPV4, when the temperature exceeds a particular threshold value (41 °C – 48 °C). This narrow temperature window currently limits the clinical application of LNS due to the potential for thermal damage to nerve bundles.

Nerve tissue cooling may be necessary during laser stimulation when dealing with sensitive peripheral nerve bundles such as the vagus nerve. For this reason, the aim was to examine the operating status of the laser source (1505 nm) to be used for LNS in modulated mode. Moreover, laser energy was analyzed for both continuous-wave and modulated modes. As shown in Figure 6, a fourteen-legged butterfly package-type diode laser is driven with three drivers: One driver is for the thermoelectric cooler controller; one driver is for the optical oscillator; one driver is for the optical signal amplifier. The optical oscillator driver can be externally triggered, allowing the diode laser to operate in continuous-wave and modulated modes at a repetition rate of up to 1 kHz.

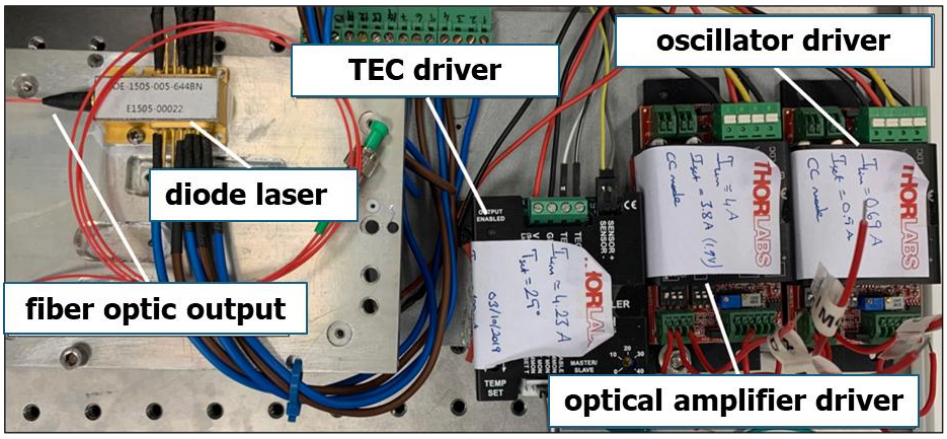



**Figure 6.** A 500 mW, single-mode fiber-coupled diode laser that produces a laser beam at a wavelength of 1505 nm. The diode laser is driven with three drivers.

Figure 7 shows the experimental setup. A function generator (DS345, SRS, USA) provided electrical square signals to modulate the optical oscillator driver, and a power meter measured optical power to estimate the laser energy and make direct comparisons between continuous-wave and modulated laser operating modes.

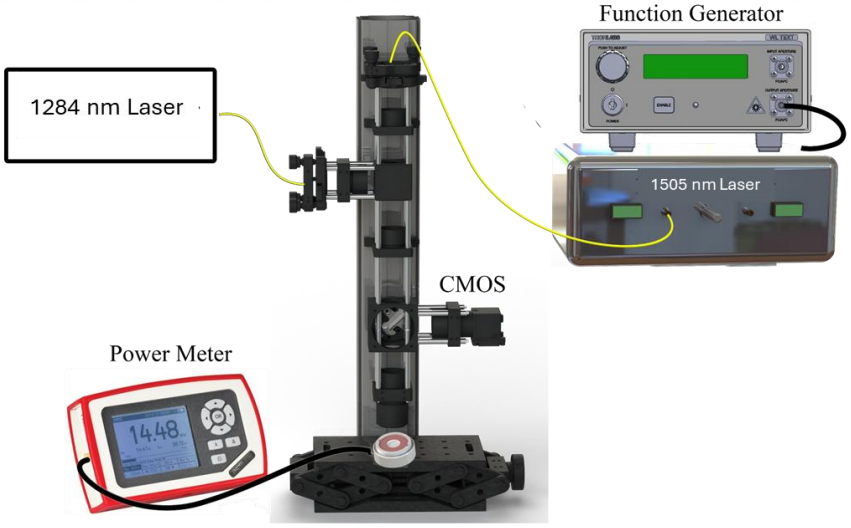



**Figure 7.** The probe operating at 1284-nm center wavelength for OCT, 1505 nm wavelength laser for LNS and CMOS for visible wavelength.The function generator is directly connected to the optical oscillator driver of the 1.505 μm wavelength laser for LNS. Lasers can be operated in continuous waveform or pulse form driven by square wave electrical signals.

### *3.6.5 Construction of the Custom-designed Modular Scanning Head*

The aim is to monitor tissue temperature changes while stimulating the vagus nerve using near-infrared laser energy. A custom-designed modular scanning head (optical probe) could be a platform combining LNS and OCT beams for this purpose.

Computer simulations were conducted to design the optical probe using a simulation package (free version 3DOptix, Israel). Figure 8 shows transient simulation results (A) and an example of CAD drawings (B). Commercially available optical components, such as lenses and mirrors, were used in the simulation. Yellow-colored rays mark the visible wavelength, orange-colored rays mark the 1505 nm wavelength, whereas red-colored rays mark the 1284 nm wavelength.

An achromatic lens with a focal length of 40 mm focused the 1505 nm laser beam on a dichromatic mirror, while another lens with a focal length of 30 mm focused the 1284 nm OCT beam on the same mirror. A 25 mm focal length bi-convex lens was an optical relay; other lenses collected and directed visible and near-infrared beams. The simulation estimated an optical loss of approximately 12% in the visible range and 35% in the near-infrared range. The optical probe had surface scanning ability in a single axis at a rate of 1 kHz, covering a 4 mm range. The scanning lens used provided a scanning area of 9.4 x 9.4 $mm^2$. Figure 8C shows the custom-designed modular scanning head (optical probe).

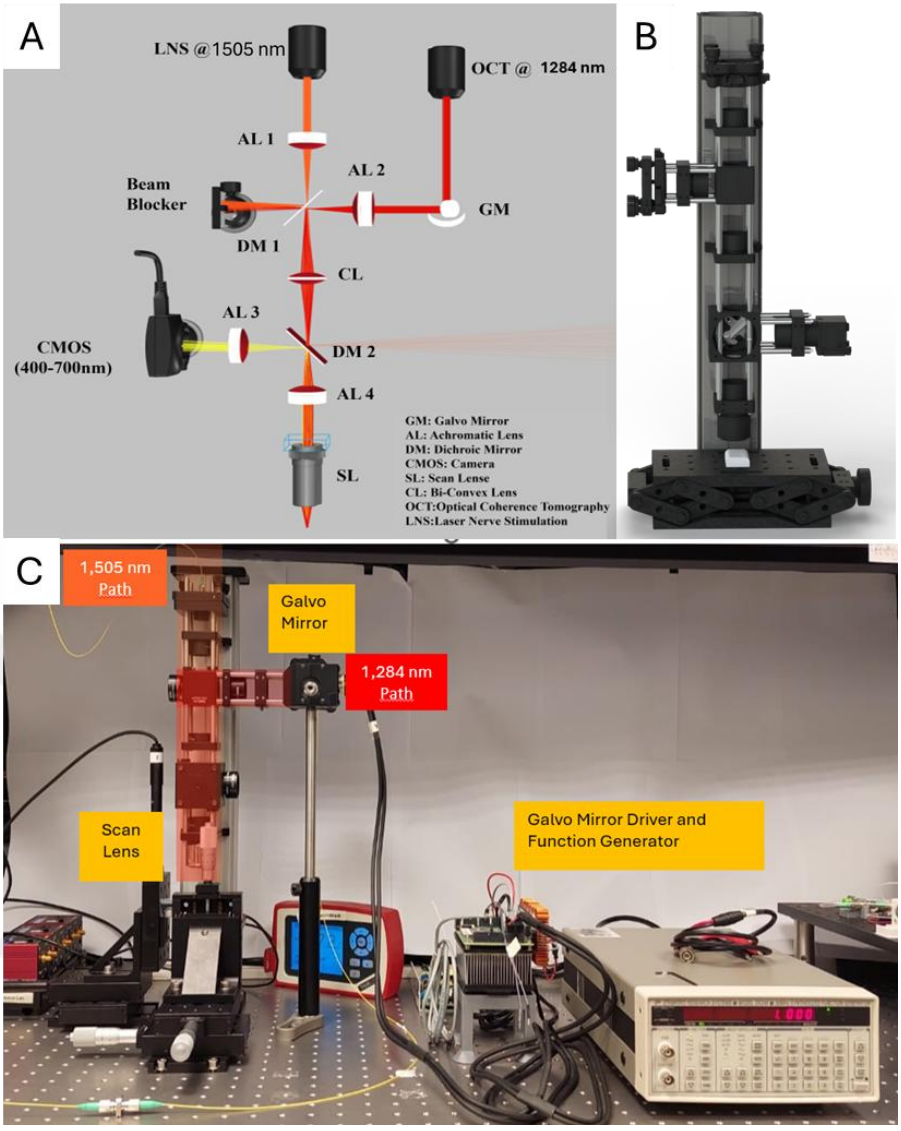



**Figure 8. (A)** Beam optics simulation results of the probe design. **(B)** Custom-designed microscope. **(C)** Optical insertion loss was estimated at ~12% in the visible and ~35% in the near-infrared range.

Figure 9 shows a schematic of the setup that measures laser power as a function of the electric current applied to the diode chip. The experiment used a near-infrared optical sensor (S122C, Thorlabs, USA) and an attached power meter (PM100D, Thorlabs, USA). Since the sensor's manufacturer-specified damage threshold is 40 mW, an absorption-based filter (NE10A, Thorlabs, USA) was added to the setup to prevent any optical damage.

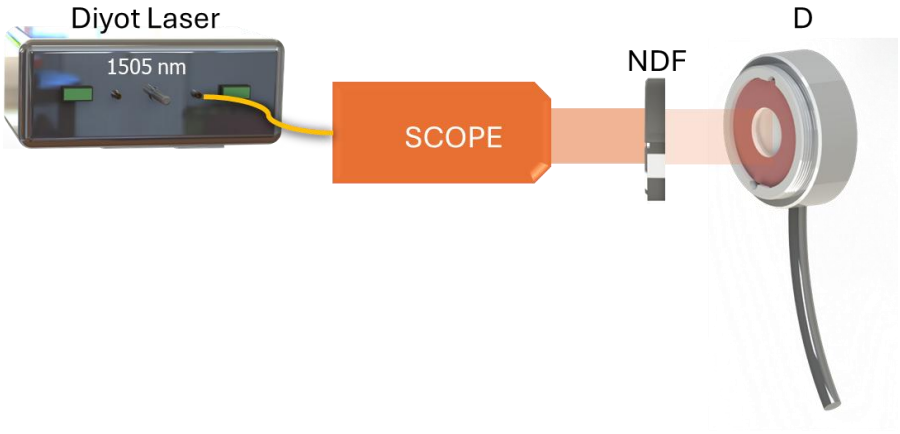



**Figure 9.** Block diagram of the laser power measurement setup. NDF: Neutral density filter. D: Sensor.

### *3.6.6 Beam Waist Measurements Using Knife-edge Method*

Determining the diameter of the laser beams (LNS at 1505 nm and OCT at 1284 nm) is essential for accurately calculating laser energy density in safe, reliable, and reproducible OCT-guided LNS. Maintaining the beam diameter over the surface during surface scanning also plays a critical role in monitoring the nerve's depth-resolved temperature change. Thus, the knife-edge method was used as a standard and affordable way of measuring the beam diameter. Figure 10 demonstrates the experimental setup used in the laser beam radius (i.e., laser beam waist) measurements focused with the optical probe at different scanning points along the surface.

A razor blade blocks the laser beam from different distances in the measurement. Laser power was acquired at every point of the razor. Then, the waist of the laser beam under test was calculated using a Gaussian fit to the measured laser powers. The change in the laser beam waist (if any) can be estimated by repeating the measurements and calculations for each spot over the surface.

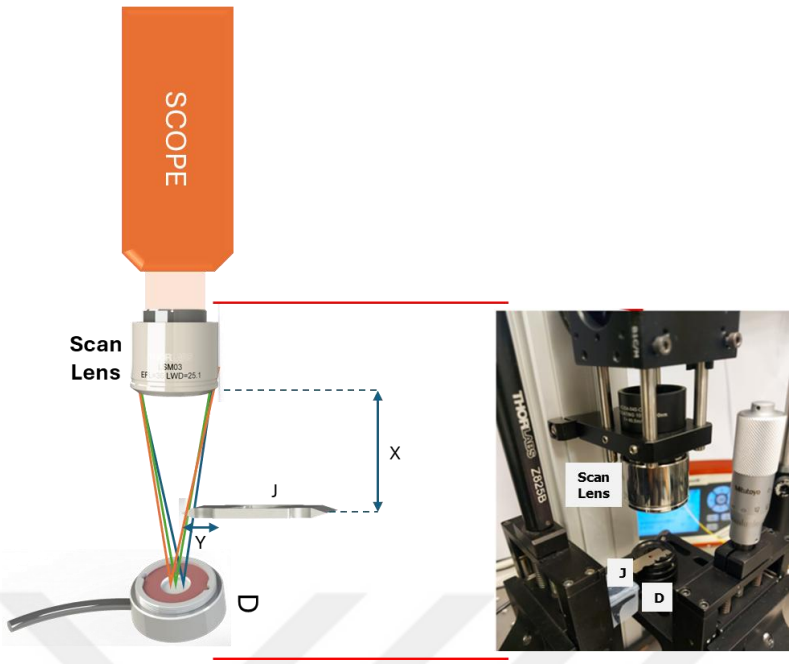



**Figure 10.** Schematic of the knife edge measurement technique to measure the beam waist focused by the probe. D: Sensor. J: Sharp-edged razor.

In the case of LNS, the laser beam at 1.505 µm wavelength was focused on a single point, as shown in Figure 11. Besides, the OCT beam at 1.284 µm was scanned using a galvo mirror driven with different direct voltages at 0 Hz. Therefore, the beam under test was focused on the fixed spot. In both cases, a single-axis stage using a motorized actuator moves the razor with a step size of 0.01 mm along the y-axis.

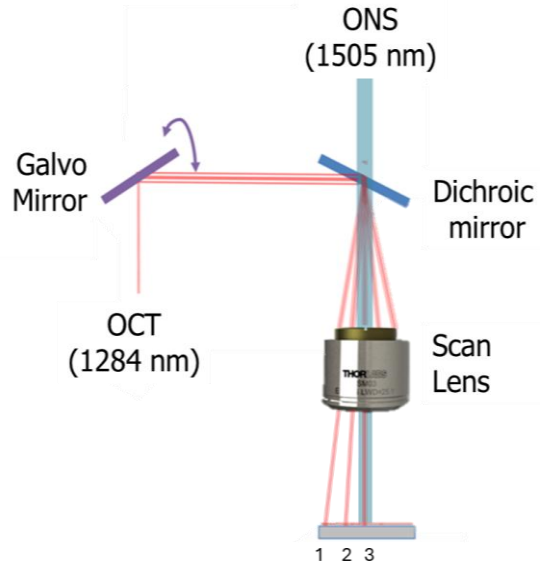



**Figure 11.** Diagram of the knife-edge measurement technique for measuring the waist of light scanned by the Galvo Mirror.

The laser beam radius (beam waist) was calculated using the measured laser power and the following equation:

$$P = P_0 + \frac{Pmax}{2}(1 - \left(\frac{\sqrt{2}(y - y_0)}{W}\right))$$

where $P_0$ is the instant laser power, $P_{max}$ is the maximum power, $y_0$ is the starting position, erf is the standard error function, and w is the calculated beam waist.

### *3.6.7 Characterization of the Surface Scanning Performance*

The scanning performance of the galvo mirror was examined using a visible diode laser operated at 660 nm. An experimental setup (Figure 12A), including a mirror holder (Figure 12B), measured scanning distances as a function of the applied voltage. This analysis was detailed by changing the scan rate from 10 Hz to 2 kHz with a step size of 200 Hz. Some examples of surface scans are shown in Figure 12C.

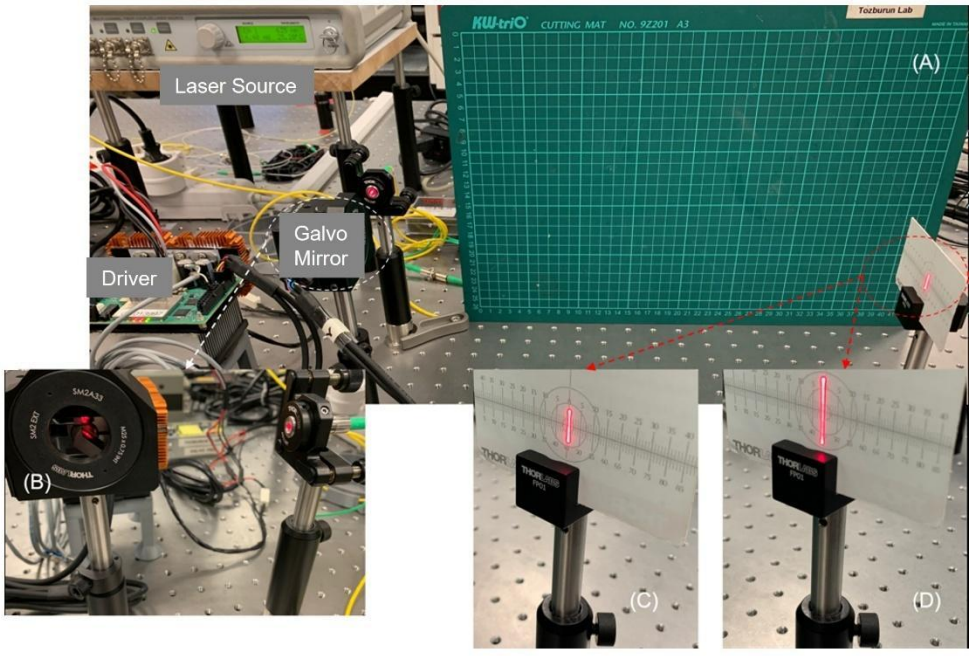



**Figure 12. (A)** The mechanism in which the scanning mirror is calibrated. **(B)** Specially designed mirror holder. **(C)** Scanning distances at 1 kHz can be adjusted depending on the amplitude of the electrical signal.

### *3.6.8 Integrating Laser Beams, CMOS and Thermal Cameras*

This part of the work aims to integrate laser outputs and a CMOS camera into the modular scanning head (i.e., optical probe). The probe aligns laser beams at 1284 nm (OCT) wavelengths and 1505 nm (LNS) on the sample and focuses them on the same point. The design includes a CMOS camera to observe neural tissue via real-time white-light imaging. Besides, the camera provides any color change in gross anatomy, corresponding to thermally induced visual changes in tissue.

On the other hand, a thermal camera (XI400, Optris GmbH, Berlin, Germany) was externally added to visualize the surface temperature of the nerve feedback. Figure 13 shows a photograph of the final iteration of the modular scanning head and externally included thermal camera.

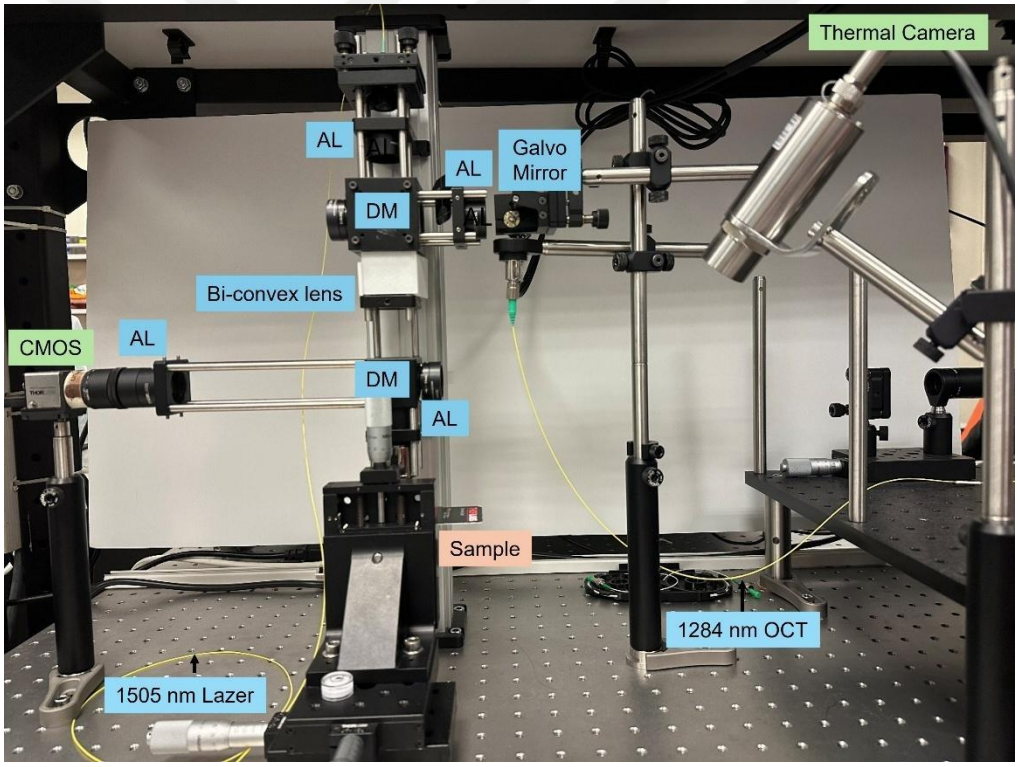



**Figure 13.** Photograph of the final version of the modular scanning head and externally included thermal camera.

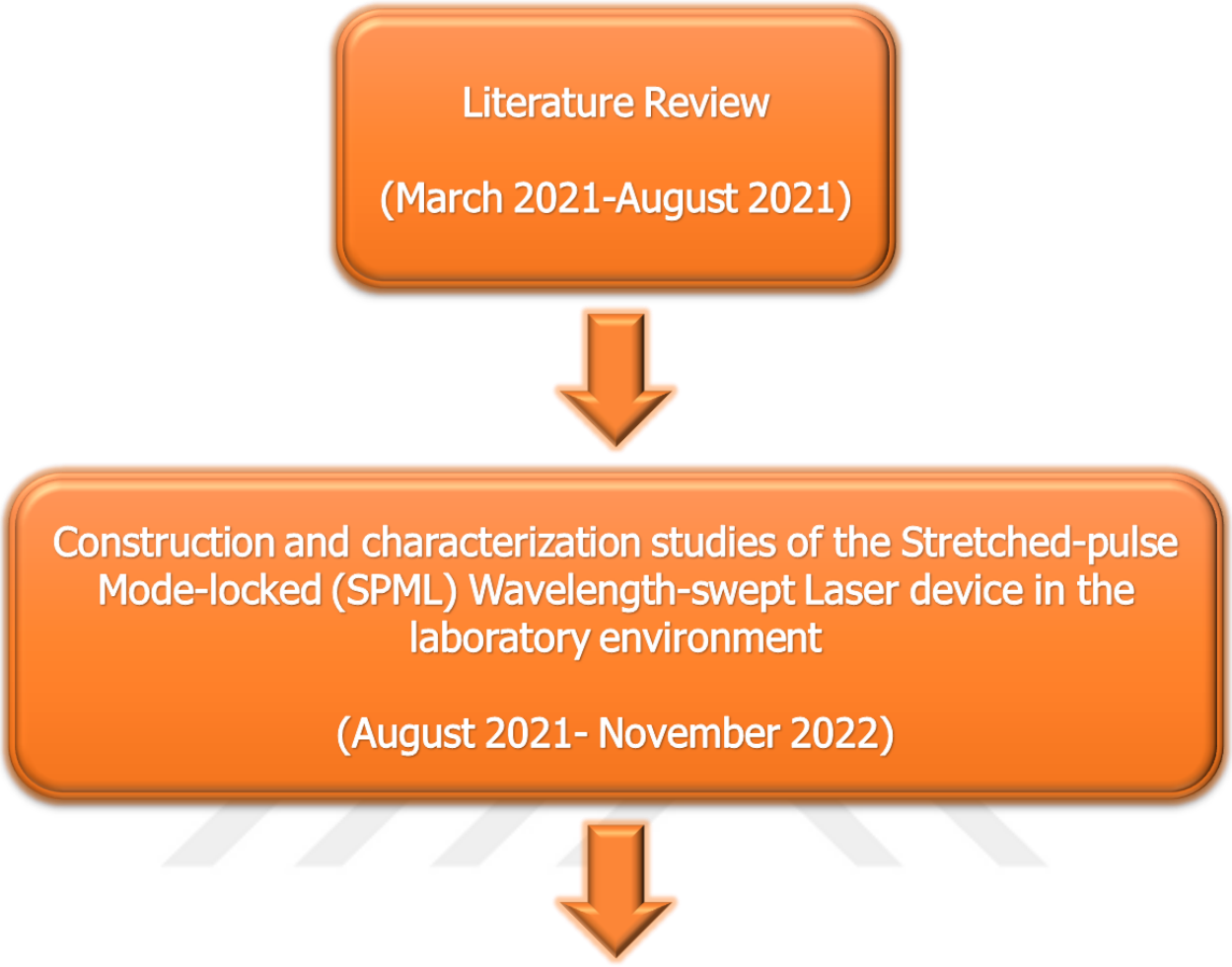
### *3.6.9 Preparation of An Agar Phantom*

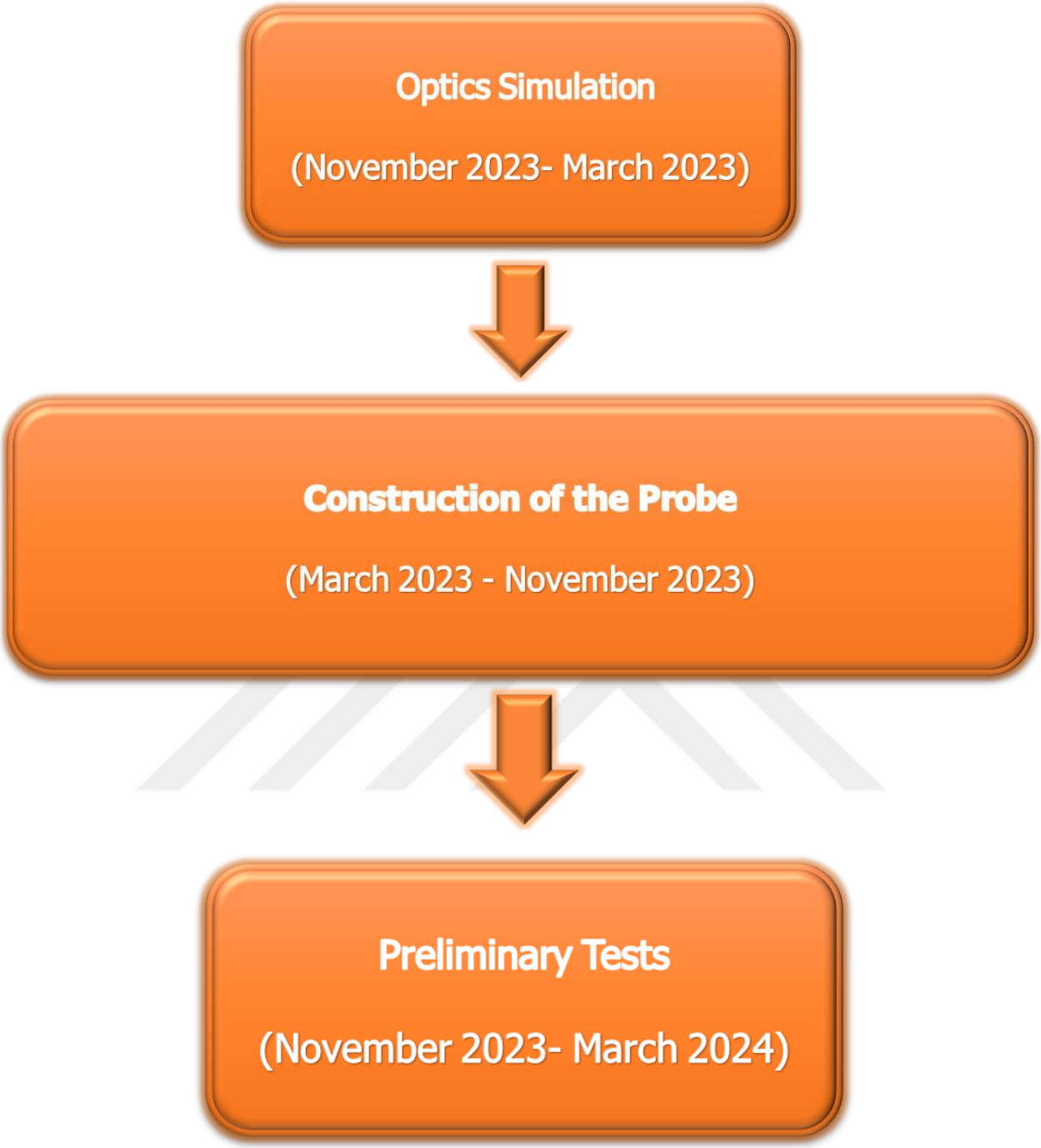
The imitation of soft tissue called agar phantom was prepared using ingredients like agar powder, lard, water, NaCl (salt), and sodium benzoate [6]. Table 1 shows the amount of each ingredient used to create 100 ml of the phantom. NaCl and sodium benzoate were mixed in distilled water and heated until boiled, and agar powder was slowly added while stirring for 10 minutes. While keeping it warm, melted lard was poured until the mixture became smooth, creamy, and opaque. Finally, this mixture was kept at +4 °C overnight. Prepared phantoms were rested at room temperature for at least 1 hour before measurements.

**Table 1.** Ingredients and quantities used in a 100 ml agar-based phantom.

| | Lard (ml) | Water (ml) | NaCL (g) | Sodium benzoate (g) | Agar (g) |
|---|---|---|---|---|---|
| Gland | 40 | 60 | 0.6 (1%) | 0.06 (0.1%) | 1.8 (3%) |

### 3.7. Research Plan




Optics Simulation
(November 2023- March 2023)
Construction of the Probe
(March 2023 - November 2023)
Preliminary Tests
(November 2023- March 2024)

### 3.8. Data Evaluation

Data were analyzed and plotted using 3DOptix software.

### 3.9. Limitations of the Study

The coherence length of the run depends on the bandwidth of the balanced detector. In order for the system to make more detailed and comprehensive measurements, a photodetector with higher bandwidth needs to be developed.

Future research should focus on using the OCT capabilities of the laser on biological tissues. In this study, melting was observed in the phantom exposed to a laser for a long time. This limited the OCT coherence length. Biological samples that do not produce volumetric changes within a narrow temperature range should be identified. Thus, the temperature increase that the laser will create in biological tissue will not limit OCT performance.

The oscilloscope with a sampling rate of 40 GS/s used in this study could not record long-term laser exposure of the biological sample. Therefore, it creates a dependency on high-speed data acquisition cards for uninterrupted operation.

### 3.10. Ethics Approval

This study was approved by the Non-Invasive Research Ethical Committee of IBG with the protocol number 2021-045 on 12/31/2021. The thesis approval is presented in section appendix.

# 4. RESULTS

## 4.1 Lasing Performance of the SPML Laser

The performance of the electro-optical modulator (i.e., intensity modulator) in optical pulse generation was directly dependent on the quality of the electrical signals produced by the bit generator. Therefore, the generated electrical pulses were examined. Figure 14 shows a series of measurements obtained from the bit generator as a function of the bandwidth of the RF signal generator providing the clock signal to the bit pattern generator. The bandwidth of the RF signal was varied from 1 GHz to 5 GHz in 1 GHz increments. Additionally, the bias voltage applied to the optical modulator, which is recorded at different bandwidths before each measurement, was adjusted according to the minimum optical transmittance. As expected, the narrowest optical pulse linewidth was obtained in the clock signal at 5 GHz. The pulse width was measured to be 212.8 ps, which is long enough compared to the relaxation time of the diode laser chip.

Figure 15 shows the average bias voltages applied to the optical modulator as a function of bandwidth. Three replicates were taken for each bandwidth at different periods (approximately 1 hour apart). The result indicated that the bias voltage did not increase significantly as a function of the bandwidth of the clock signal. For example, the bias voltage was between 4.10 volts and 4.20 volts at a 4-GHz clock signal, which is considered a suitable value range. Accordingly, although the bandwidth increases, the temperature of the crystal inside the optical intensity modulator does not significantly increase. Therefore, considering the repetition rate of the SPML laser, it was determined that the modulator could operate smoothly in the wide bandwidth range of clock signals. Nevertheless, just in case, a bias controller has been added to the cavity to prevent transient temperature changes and possible momentary performance fluctuations.

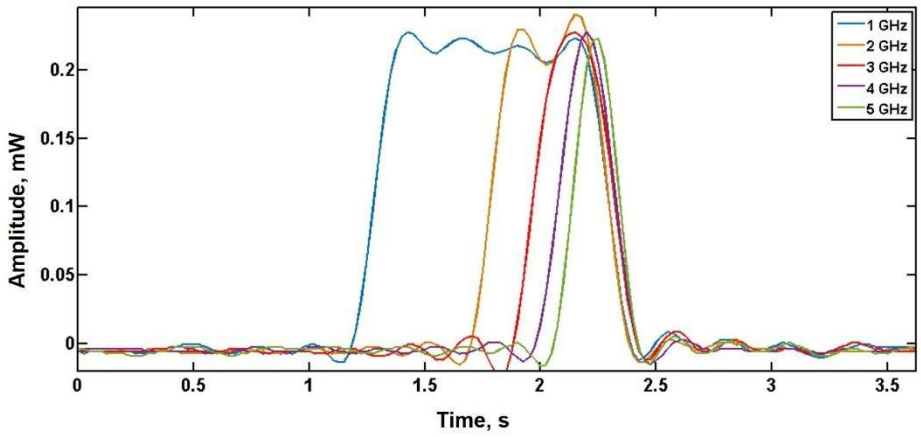



**Figure 14.** Variation of narrow electrical pulses produced by the optical amplitude modulator concerning the clock signal pulse. The narrowest linewidth was 212.8 ps.

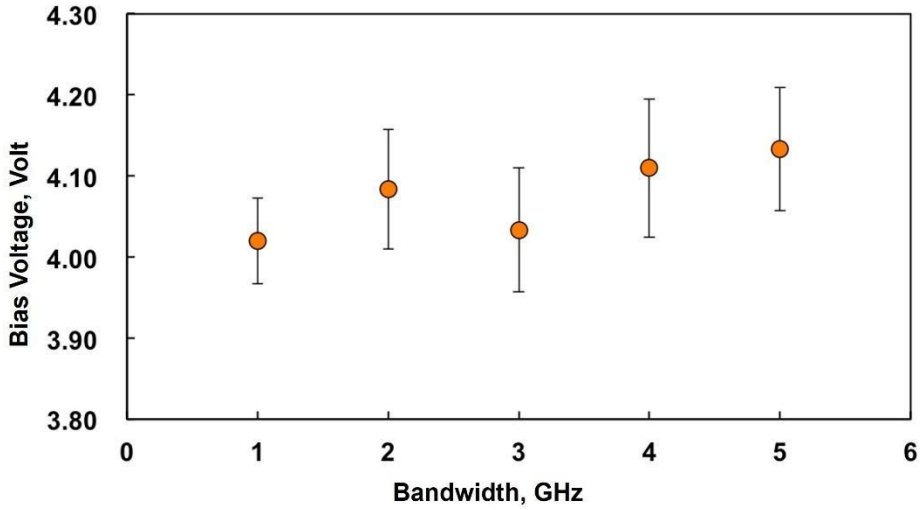



**Figure 15.** Average measurement results and standard deviation of the bias voltage applied to the amplitude modulator in each clock signal bandwidth condition. N=3.

Figure 16 shows the measured optical bandwidth of the SPML laser as 105 nm at a center wavelength of 1283.72 nm. The laser's time-domain output was detected by a high-speed photodetector (UPD-15-IR2-FC, Alphalas, Germany) and recorded by a fast oscilloscope (40 GS/s, 3.5 GHz, DPO7354C, Tektronix, USA). The repetition rate of the laser was measured as 22.70417 MHz at 88% duty cycle, as shown in Figure 17. It corresponded to the 3rd-order harmonic of the laser cavity's round-trip time. The average output power measured from a 25% tap coupler was 10.2 dBm.

Relative intensity noise (i.e., instability of the optical intensity normalized to average optical power) was measured to be -123.2 dB/Hz at 1GHz in the range of 3 GHz.

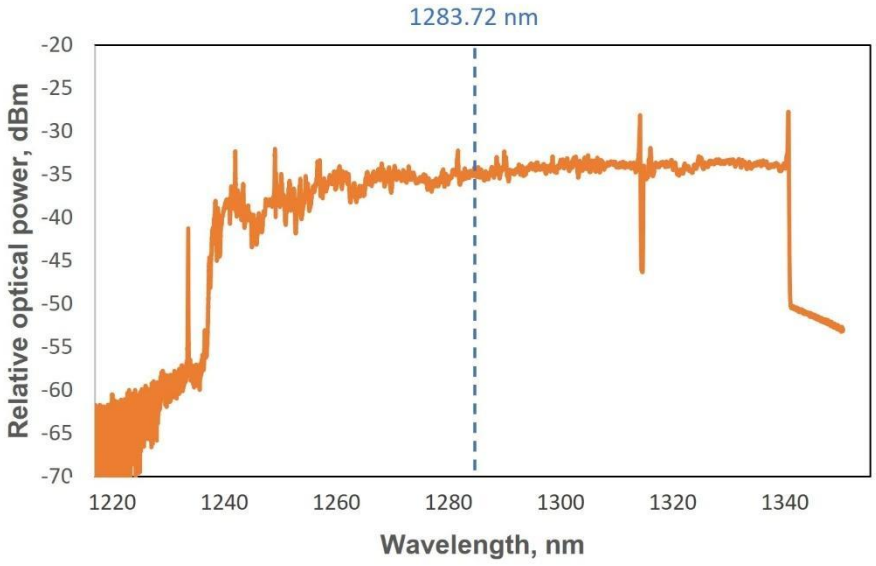



**Figure 16.** Representative spectral output of the SPML laser. The measured optical bandwidth is 105 nm at a center wavelength of 1283.72 nm.

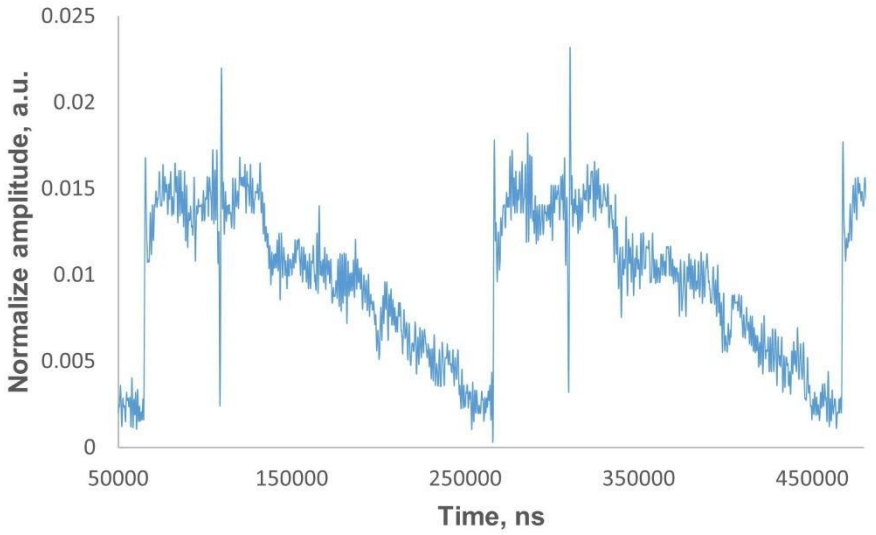



**Figure 17.** Tentative time-domain output of the SPML laser. Repetition rate of the optical pulses is 22.70417 MHz at 88% duty cycle.

### 4.2 Timing Jitter

The signal generator set the clock of the bit generator by driving the electro-optical modulator (i.e., optical density modulator), and the accuracy of the clock signals was a critical parameter of SPML laser performance in OCT applications. Thus, the clock signals were tested using a method described in Section 3.6.2.

Figure 18A shows an example of signals acquired for 625 µs using an oscilloscope at 40 GS/s. The timing jitter was estimated to be approximately 64 ps from the histogram shown in Figure 19B.

This measured jitter was in the correct range for electrical signals with a pulse width of 212.8 ps generated from the bit generator to drive the optical modulator (Figure 18B). Therefore, optical pulses < 213 ps did not experience delay or lead in the cavity due to timing jitter on the order of 64 ps.

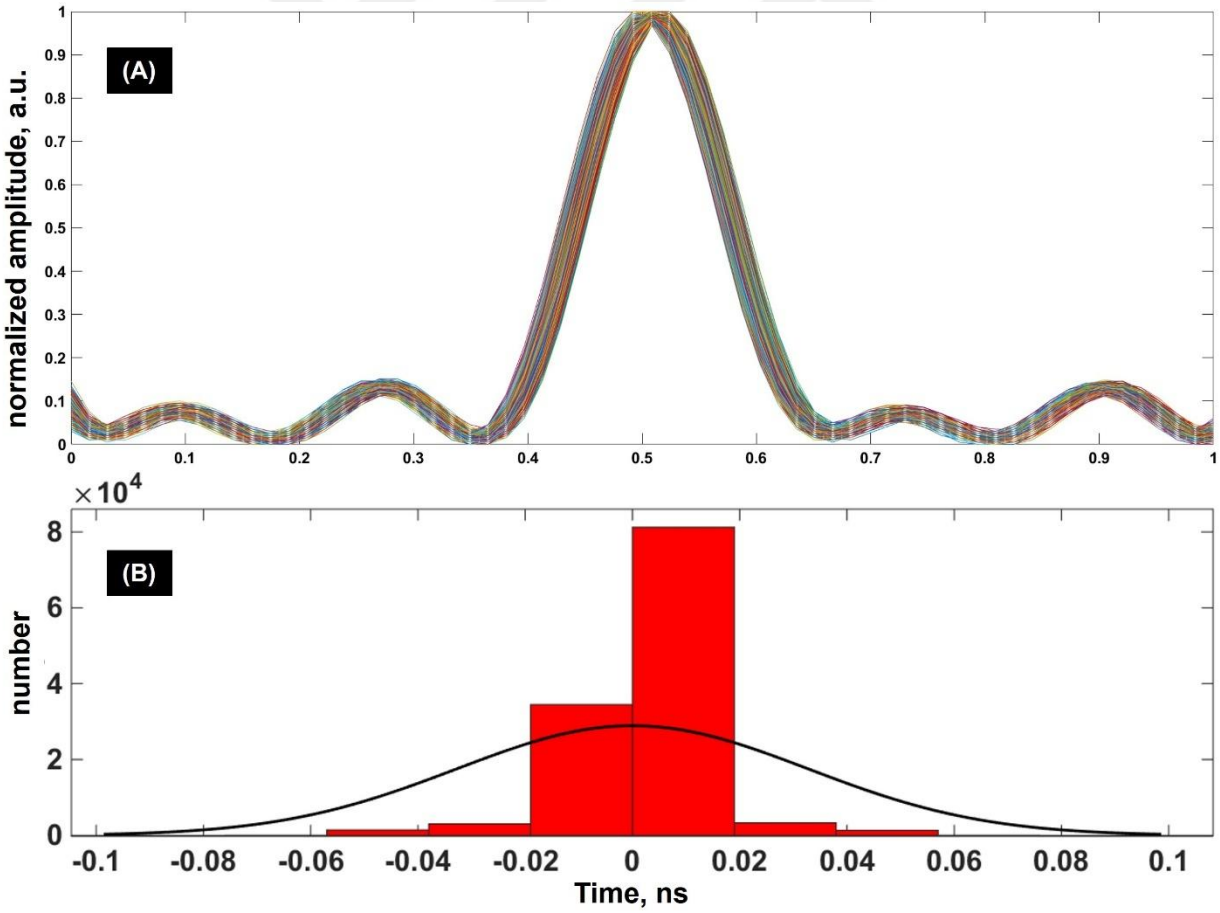



**Figure 18.** Electrical signal examples produced by the function generator are plotted on each other. The jitter/standard deviation value was measured at approximately ~3-µs at the time the generator had.

### 4.3 OCT Performance of the SPML Laser

Here, the OCT performance of the SPML laser source using a specially designed modular scanning head as the imaging probe in the interferometer was investigated. The research included two critical parameters: axial resolution and coherence length. In this study, the gold-plated mirror on the sample arm was moved gradually with a step distance of 0.1 mm. In the sample arm, an optical attenuator with an optical density of 2.0 was placed in front of the mirror, causing 40 dB insertion loss in a double-pass configuration to mimic the optical loss of the biological sample. The fringe signals were recorded for each mirror position using a fast oscilloscope at 40 GS/s (DPO7354C, Tektronix, USA). Figure 19 shows the tentative fringe signals recorded for the optical path length difference between 0.1 mm and 1.2 mm at a step size of 0.01 mm. A one-dimensional fast Fourier transform was applied to each fringe signal in the MATLAB numerical processing environment. The corresponding point spread function results are shown in Figure 20. The axial resolution was 18.1 μm in the air (i.e., FWHM of the point spread functions), comparable with the lateral resolution of the optical probe (<21 μm) at the wavelength of 1284 nm.

The coherent length of the swept-source laser was defined as the distance at which the amplitude of the point spread functions drops to a level of 1/e as a function of the optical path length difference. The laser source produced a coherence length of 0.6 mm in the single-pass configuration (1.2 mm in the double-pass configuration), as shown in Figure 20.

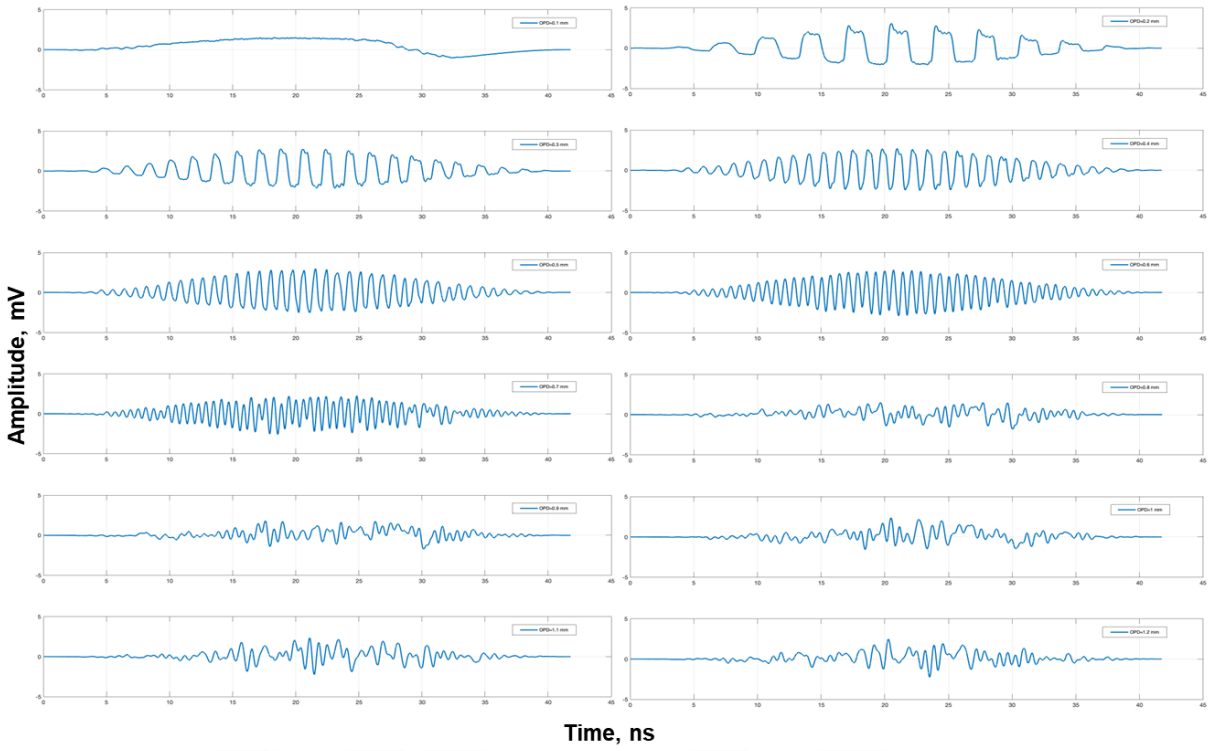



**Figure 19.** Tentative fringe signals recorded for the optical path length difference between 0.1 mm and 1.2 mm at a step size of 0.01 mm. OPD: Optical path length difference.

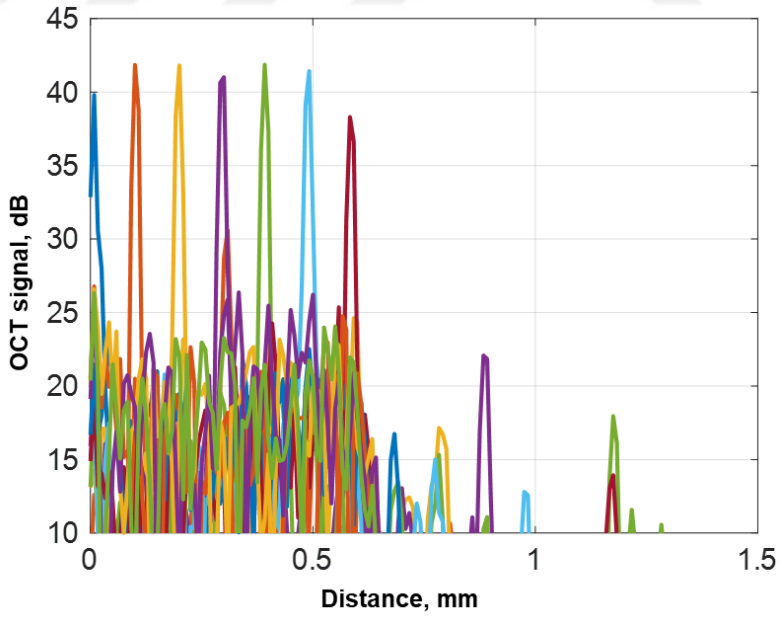



**Figure 20.** Estimated corresponding point spread functions The axial resolution was 18.1 µm in the air and the SPML laser produced a coherence length of 0.6 mm in the single-pass configuration.

### 4.4 Performance of the Custom-designed Modular Scanning Head at 1505 nm Used for LNS

Soft tissues such as nerve fibers contain 70% to 80% water and are also considered homogeneous. Therefore, water molecules are critical in converting laser energy into heat energy by absorbing near-infrared laser energy in soft tissue. Besides, the absorption coefficient in water along the near-infrared wavelength determines the optical penetration depth. The absorption coefficient (red line) and the corresponding optical population depth (blue line) along the laser wavelengths are presented in Figure 21 [12]. Thus, it was evaluated that a single-mode fiber-coupled diode laser emitting light at a wavelength of 1505 nm could provide the near-infrared laser energy needed for laser nerve stimulation.

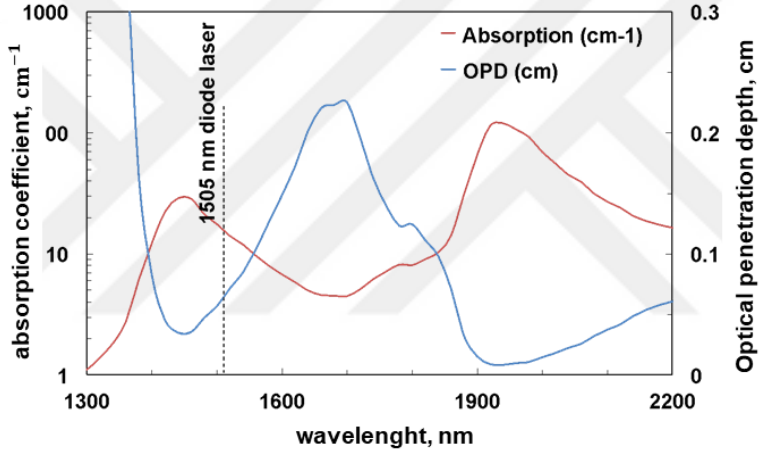



**Figure 21.** Absorption coefficient (blue line) and optical penetration depth (red line) in water along the near-infrared optical wavelength [12]. The dashed black line indicates the laser wavelength used in the study, which provides optical penetration depth that closely matches the diameters of peripheral nerves in rats.

The output powers of the custom-designed modular scanning head (i.e., optical probe) for the 1505 nm laser were measured at different electrical currents gradually increasing up to 2.0 A in 100 mA steps (Figure 22A). Figure 22B shows the laser output power values provided by the diode laser manufacturer. The optical loss caused by the probe was calculated to be around 37%.

The estimated result closely matched the power measurement trend provided by the manufacturer; this showed that the laser power output could be up to 500 mW in case of no optical loss.

On the other hand, it was observed that the laser power focused on the nerve (315 mW) was well above the estimated laser power (40-50 mW) required for successful and reliable LNS at a wavelength of 1505 nm [41]. The pink line represents how the potential difference (voltage) applied to the diode laser chip changes with electric current.

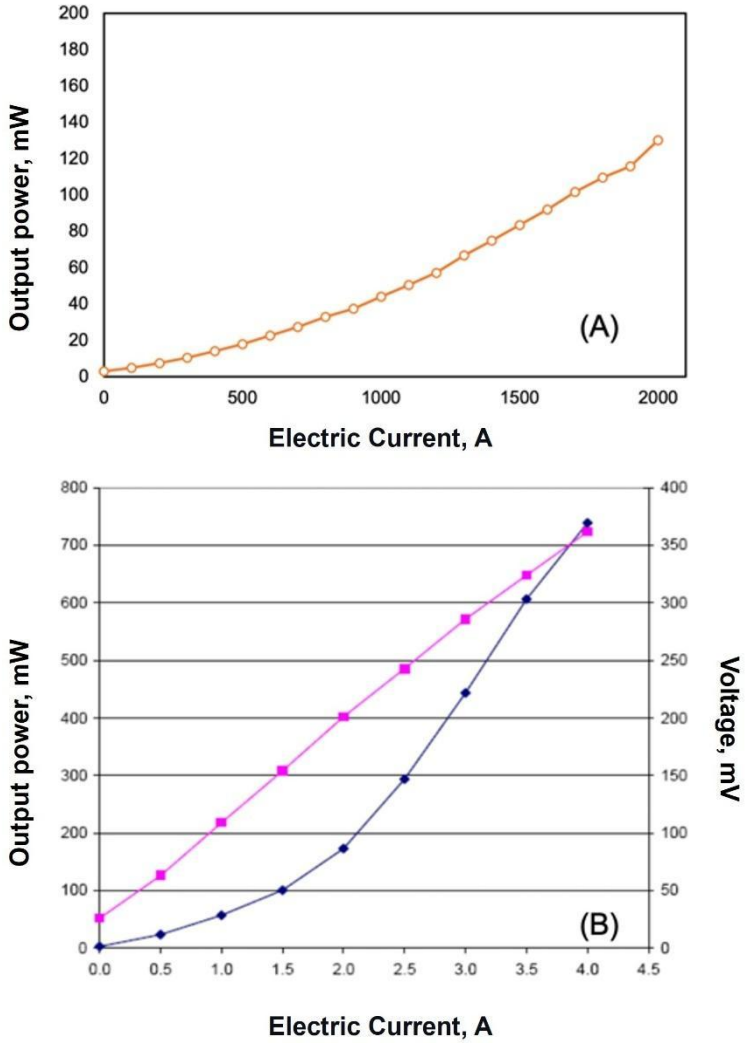



**Figure 22.** Variation of laser power according to the electric current applied to the chip of the diode laser. **(A)** Due to the limited optical damage threshold of the sensor in laboratory measurement, the electric current was scanned with a range of 100 mA increments up to a value of 2 A. **(B)** Measurement chart provided by the manufacturer. The pink line indicates the change in the potential difference (voltage) applied to the chip of the diode laser according to the electric current.

## 4.5 Beam Waist Measurements

Figure 23 summarizes the results of beam diameter (2 x beam waist, also defining lateral resolution) measurements using the knife-edge method. Here, the laser power was measured and normalized as a function of sliding a razor blade perpendicular to the beam. The Galvo mirror was driven with DC voltage, and a scanning lens (LSM03, Thorlabs, USA) focused beams at different points on the sample surface. As seen in Figure 11, the DC voltage was set to 0 Volt for position 1, 0.5 Volt for position 2, and 1.3 Volt for position 3. The 1284 nm beam diameter was 18.6 µm at position 1, 20.2 µm at position 2, and 20.4 µm at position 3, respectively. The 1505 nm beam diameter was 22.1 µm at position 1, 20.4 µm at position 2, and 19.5 µm at position 3, respectively. There was no significant difference in beam diameter between laser wavelengths. The standard deviation of the beam diameters was calculated to be 1.05 µm.

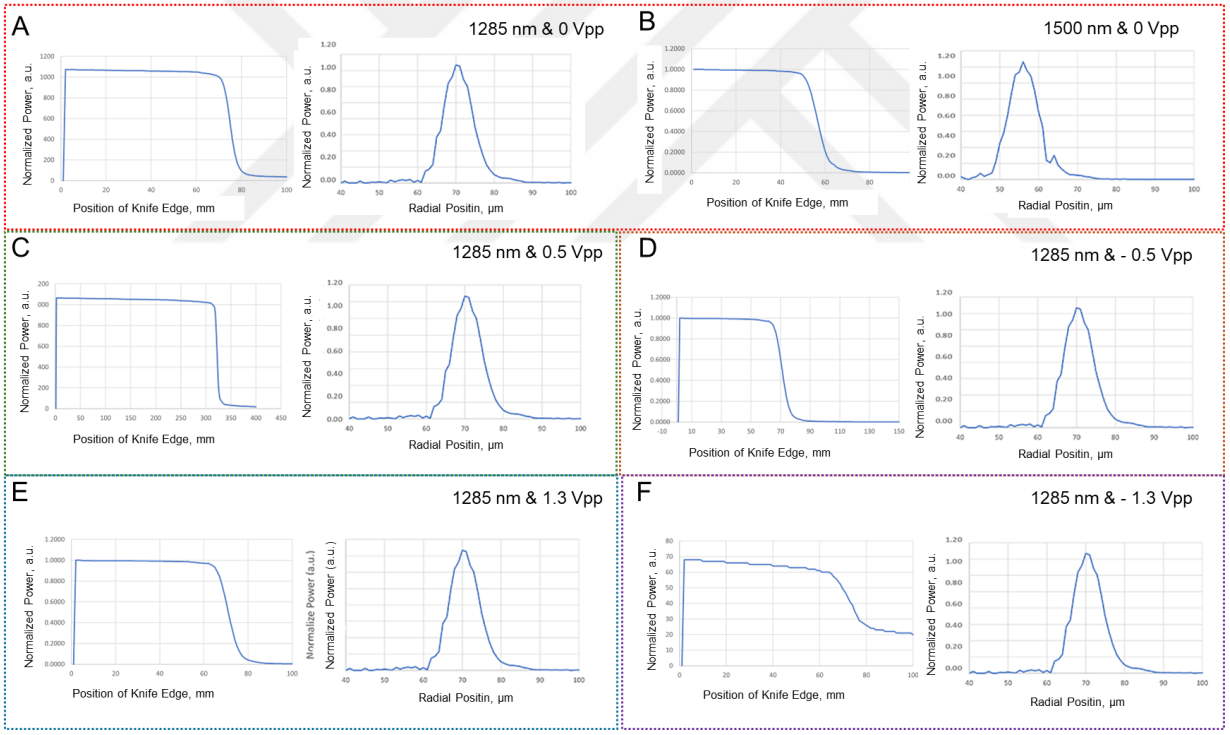



**Figure 23.** Results of beam diameter measurements. The beam diameter at position 1 (0 Volt) was 18.6 µm for 1284 nm (A) and 22.1 µm for 1505 nm (B). The beam diameter at position 2 (0.5 Volt) was 20.2 µm for 1284 nm (C) and 20.4 µm for 1505 nm (D). The beam diameter at position 3 (1.3 Volt) was 20.4 µm for 1284 nm (E) and 19.5 µm for 1505 nm (F).

### 4.6 Laser Energy Analysis of 1505 nm Laser for Continuous Wave Mode and Modulated Mode

Figure 24 displays examples of square wave signals created by the function generator, with changes in repetition rates (10 Hz to 200 Hz) and duty cycles (10%, 25%, 50%, 75%, and 90%). These results help us to understand how laser energy varies in different repetition rates and duty cycle scenarios.

Figure 25 shows the results of laser energy as a function of pulse repetition rate. Duty cycle comparison is color-coded in the figure. As expected, higher repetition rates caused pulse energy to increase, whereas when electrical signals had a constant repetition rate, longer laser pulses were produced with higher duty cycles, resulting in increased pulse energy.

The orange column represents the laser energy in continuous-wave mode for direct comparison. The results showed that continuous-wave and modulated laser operations could provide sufficient and comparable energy for safe and reliable LNS. In addition, the results indicated that the thermal effect of laser-tissue interactions may be comparable when soft tissues are exposed to a laser beam in quasi-continuous (i.e., modulated mode) or continuous wave mode.

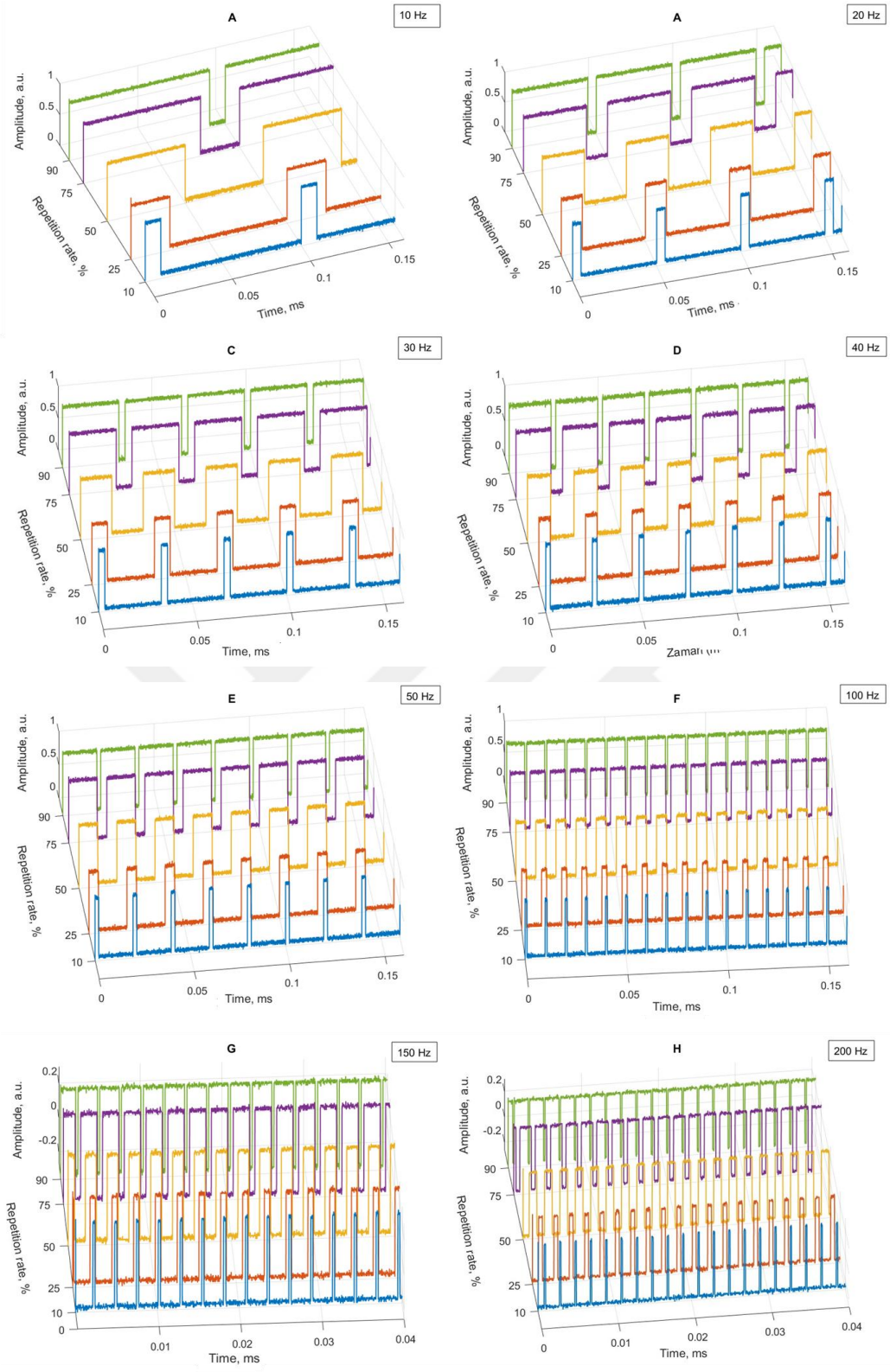



**Figure 24**. Examples of square wave signals the function generator produces at different duty cycles (10%, 25%, 50%, 75%, 90%). **(A)** 10 Hz repetition rate. **(B)** 20 Hz repetition rate. **(C)** 30 Hz repetition rate. **(D)** 40 Hz repetition rate. **(E)** 50 Hz repetition rate. **(F)** 100 Hz repetition rate. **(H)** 150 Hz repetition rate. **(G)** 200 Hz repetition rate.

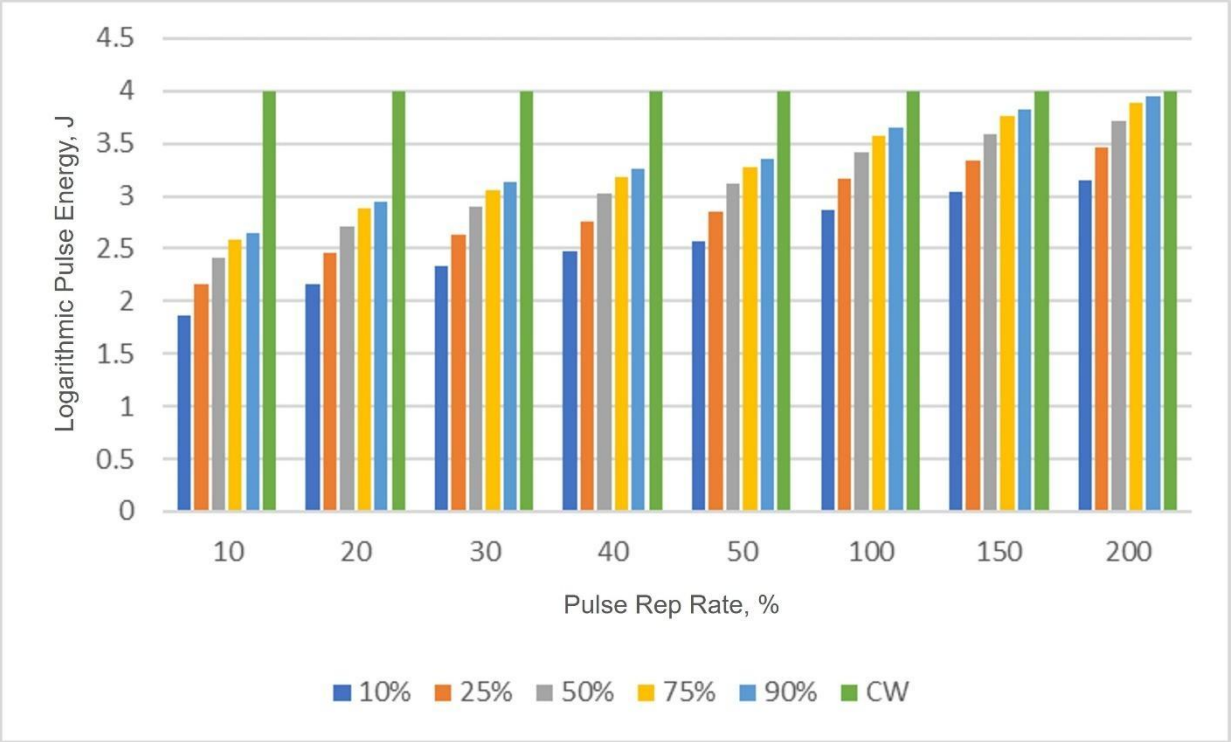



**Figure 25.** Determined laser energy for different repetition rates and duty cycles. The laser energy produced in the continuous wave case is also placed in the graph with an orange column for direct comparison.

### 4.7 Integrating Thermal and Digital Cameras

Figure 26 shows images of an IR card captured with a CMOS camera during 1284 nm laser irradiation (A) and 1505 nm laser irradiation (B). To visualize the alignment of two laser beams transmitted through different optical paths, the image in Panel A was presented in the green channel and the image in Panel B was presented in the red channel and then were superimposed.

Panel C shows a representative superimposed image. An open-source image processing program called ImageJ was utilized in this part of the study. The yellowish color appears more prominent and indicates significant overlap of images as well as focal points. Additionally, pixel-based analysis was performed between Panel A and Panel B. The estimated overlap rate was >98%.

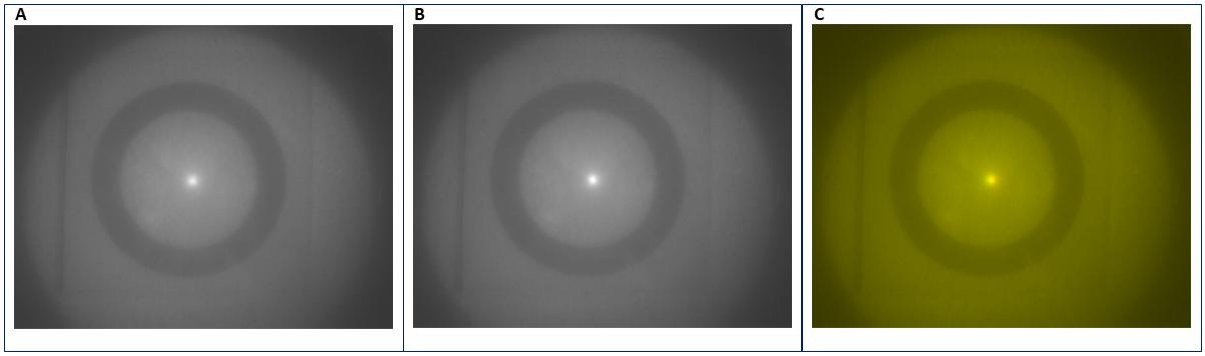



**Figure 26. (A)** Image of an IR card captured with a CMOS camera during 1284 nm laser irradiation. **(B)** Image of an IR card captured with a CMOS camera during 1505 nm laser irradiation. **(C)** Representative superimposed image.

### 4.8 Phantom Trials of the Integrated System

The system, consisting of a 1284 nm SPML laser, a 1505 nm laser, the custom-designed modular scanning head, and digital and thermal cameras, was tested in an agar phantom. Figure 27A shows an example of a produced fringe signal (i.e., OCT signal) from a single point on the sample (agar phantom). Figure 27B shows real-time imaging using a CMOS camera in the visible range at 30 fps. The greyscale video capability was used for alignment purposes and visualization of any thermal-damage-induced structural changes on the sample surface during 1505 nm laser irradiation. A thermal camera (XI400, Optris GmbH, Berlin, Germany) measured the sample's surface temperature at 30 frames per second during irradiation to calibrate temperature changes. The thermal camera was externally positioned at an angle to the optical probe's path (Figure 27C).

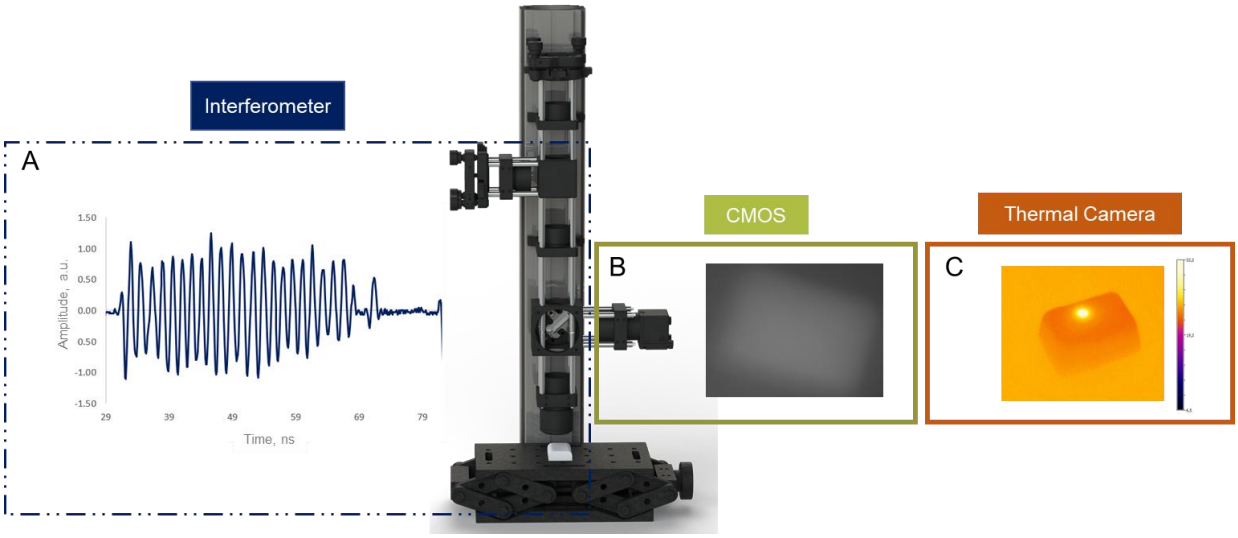



**Figure 27. (A)** An example of a produced fringe signal (i.e., OCT signal) from a single point on the sample. **(B)** Real-time imaging using a CMOS camera in the visible range at 30 fps. **(C)** Tentative thermal camera view of the sample during laser irradiation.

Figure 28 highlights the depth-resolved amplitude changes of fringe signals (OCT signals) before, during, and after 1500 nm laser exposure at different surface temperatures (22°C, 45°C, and 22°C measured by the thermal camera). Fringe signals were acquired in M-mode. The results indicated that potential changes in the sample's optical properties around 45 °C caused changes in the signals' amplitudes as a function of depth. On the other hand, the change in signal amplitude towards depth showed that the tissue was cooling from the surface to the depths. The results indicated that the system was able to capture potential changes in the sample's optical properties around 45 °C, which caused changes in the signals' amplitudes as a function of depth.

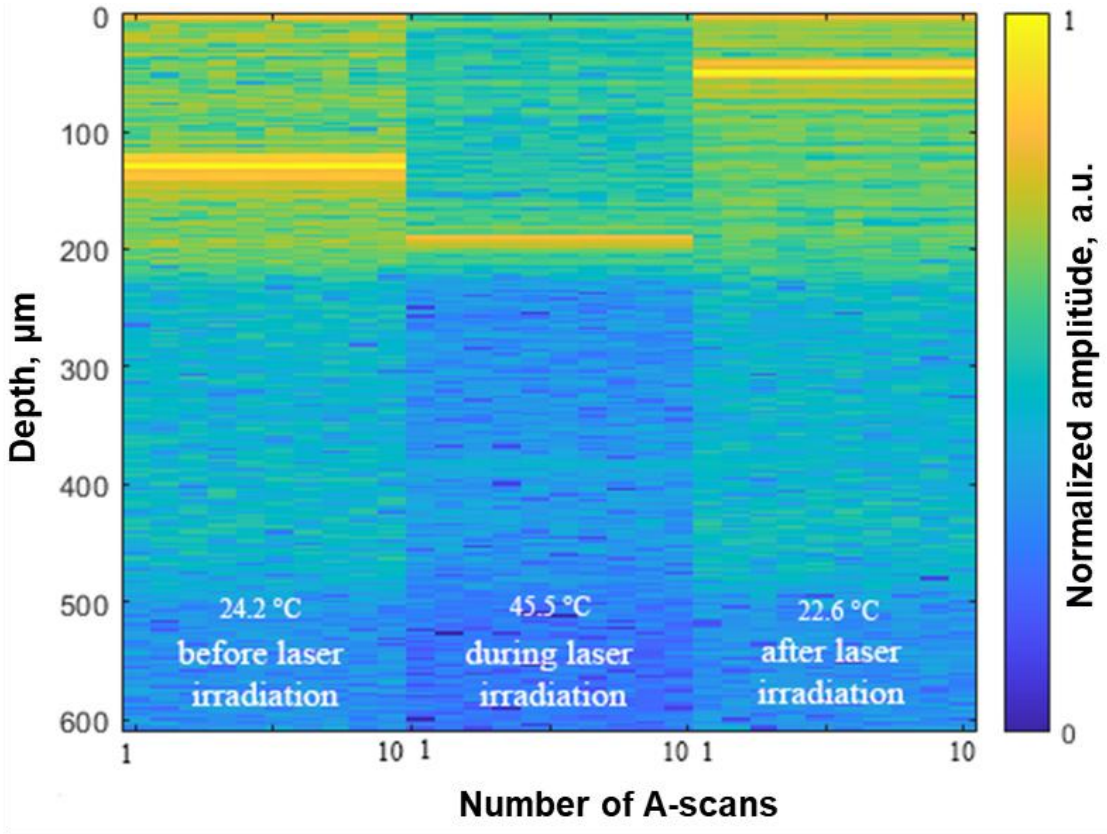



**Figure 28.** Depth-resolved amplitude changes of fringe signals (OCT signals) before, during, and after 1500 nm laser exposure. Thermal camera measured the surface temperature as 22°C, 45°C, and 22°C, respectively.

## 5. DISCUSSION

The laser nerve stimulation (LNS) technique is an emerging stimulation method that has some advantages, such as non-invasive nerve stimulation, improved spatial selectivity, and elimination of measurement errors caused by electrical interference in measurements. This stimulation technique, resulting from the thermal effect of laser irradiation-induced nerve firing, shows potential as an alternative to the traditional electrical nerve stimulation technique. However, maintaining nerve temperature within a narrow range (41°C–48°C) for safe, reliable, and reproducible LNS remains methodologically challenging. A temperature-controlled system that measures surface and depth could offer a platform to meet this challenge.

This thesis was planned to investigate the depth-resolved thermal analysis performance of a custom-designed modular scanning head (i.e., optical probe) integrating swept-source optical coherence tomography (OCT) at 1.284 μm center wavelength, 1505 nm laser for LNS, and digital camera for visualization. The lasing bandwidth of the Stretched-pulse Mode-locked (SPML) laser-based OCT was measured to be 105 nm at a sweep rate of 22.7 MHz. The system, which acquired the fringe signal in M-mode, successfully measured the change in fringe amplitude when the surface temperature increased from 22°C to 45°C in the phantom model.

This thesis demonstrates several limitations beyond its scope and should be discussed in future research. First, effective polarization control in the SPML laser cavity must be done to prevent polarization-induced loss and sensitivities mainly caused by FBGs written on standard single-mode fibers [42].

Second, although the coherence length (that is < 1 mm) of the OCT system seems relatively short, considering current demands in laser stimulation, the imaging depth is limited by the bandwidth of the balanced detector (1.6 GHz) used in the study. The coherence length provided by the laser can be examined by adding a Fabry-Perot etalon to the cavity.

Third, further investigation of the probe's capabilities must be completed in preclinical studies. For this objective, the system in its current form requires a high-speed data acquisition card coupled with a large amount of random-access memory.

Finally, apart from the highly matched chirped-FBGs, other fiber components of the SPML laser caused a dispersion of − 0.8 ps/nm. This relatively low dispersion, ignored in this study, can be eliminated by counting a compensator to the cavity.

## 6. CONCLUSION AND FUTURE DIRECTIONS

The culmination of this research effort marks a significant milestone in the development of Laser Nerve Stimulation (LNS) techniques through the integration of swept-source Optical Coherence Tomography (OCT). When reflecting on the insights gained and the challenges addressed, it is imperative to acknowledge the contributions made and chart the course for future research in neuromodulation/neurostimulation.

The integration of swept-source OCT at the 1284 nm center wavelength, 1505 nm laser, and a digital camera has remarkable capabilities for OCT-guided LNS. The successful measurement of fringe amplitude changes with varying surface temperatures in the phantom model highlights the system's sensitivity and adaptability. The study also shows that the system has the potential for depth-resolved thermal analysis of the nerve tissue during laser stimulation of the nerves in pre-clinical models. However, it is vital to acknowledge the limitations described in the study and the issues requiring further improvement.

Future studies addressing the highlighted limitations should prioritize improving the polarization control system within the cavity. Improving this feature will provide a more stable and reliable OCT system by reducing polarization-induced loss and sensitivity.

Recognizing that the imaging length depends on the bandwidth of the balanced detector underscores the need for further research. Extending the imaging length can leverage the system's depth-resolved thermal analysis capacity for more detailed and comprehensive measurements.

The transition from a phantom model to a pre-clinical model is rational. This step will require the integration of high-speed data acquisition cards and significant amounts of random access memory to acquire seconds of fringe signals (OCT signals).

The system characterized based on this study's findings should be evaluated for a phantom model. Optimization through stimulation of peripheral nerves in a pre-clinical animal model, in vivo, will provide insight into the usefulness and effectiveness of the probe, which forms the critical component of the system. It will also serve as leverage in producing results that contribute to laser nerve stimulation studies.

In conclusion, incorporating swept-source OCT using an SPML laser into the laser nerve stimulation offers a potentially transformative method for monitoring depth-resolved temperature change and understanding laser-induced thermal effects during nerve stimulation. This innovative technology may promise to reshape the laser nerve stimulation

technique and open new dimensions in neural modulation and therapeutic interventions.

## 7.References


[1] Effectiveness of transcutaneous electrical nerve stimulation for treatment of hyperalgesia and pain | Current Rheumatology Reports, (n.d.). https://link.springer.com/article/10.1007/s11926-008-0080-z (accessed January 17, 2024).

[2] Pulsed laser versus electrical energy for peripheral nerve stimulation - ScienceDirect, (n.d.). https://www.sciencedirect.com/science/article/pii/S016502700700146X?casa_token=XF0jS5JcIHcAAAAA:UUgD3OdVS6dtPra1gSVaE_Yidlj5_67yypBUa05YU5OpX76fbM_o3R_Q7UOcdwIVT_k2MvtfEMOI (accessed January 17, 2024).

[3] Using TENS for pain control: the state of the evidence | Pain Management, (n.d.). https://www.futuremedicine.com/doi/abs/10.2217/pmt.14.13 (accessed January 17, 2024).

[4] SciELO - Brazil - Electrical Stimulation for Urinary Incontinence in Women: A Systematic Review Electrical Stimulation for Urinary Incontinence in Women: A Systematic Review, (n.d.). https://www.scielo.br/j/ibju/a/cDc78mJS8z9dv5SL69wRQYp/?lang=en&format=html (accessed January 17, 2024).

[5] Review: Deep brain stimulation in Parkinson's disease - S.J. Groiss, L. Wojtecki, M. Südmeyer, A. Schnitzler, 2009, (n.d.). https://journals.sagepub.com/doi/abs/10.1177/1756285609339382 (accessed January 17, 2024).

[6] J.L. Corning and vagal nerve stimulation for seizures in the 1880s | Neurology, (n.d.). https://www.neurology.org/doi/full/10.1212/WNL.58.3.452?casa_token=VuM0q4gjXTkAAAAA%3A7_feTWBk7xKvkz8yPm-T83PYuyEe4IA9UNOC8Anta0A9x6-RNJg0oHetyAWHlw6eucox2lxjYGVyV8bv (accessed January 17, 2024).

[7] A SENSORY CORTICAL REPRESENTATION OF THE VAGUS NERVE: WITH A NOTE ON THE EFFECTS OF LOW BLOOD PRESSURE ON THE CORTICAL ELECTROGRAM | Journal of Neurophysiology, (n.d.). https://journals.physiology.org/doi/abs/10.1152/jn.1938.1.5.405 (accessed January 17, 2024).

[8] Reduction of Pentylenetetrazole-Induced Seizure Activity in Awake Rats by Seizure-Triggered Trigeminal Nerve Stimulation | Journal of Neuroscience, (n.d.). https://www.jneurosci.org/content/20/21/8160.short (accessed January 17, 2024).

[9] Inhibition of Experimental Seizures in Canines by Repetitive Vagal Stimulation - Zabara - 1992 - Epilepsia - Wiley Online Library, (n.d.). https://onlinelibrary.wiley.com/doi/abs/10.1111/j.1528-1157.1992.tb01751.x (accessed January 17, 2024).

[10] Prevention of Intractable Partial Seizures by Intermittent Vagal Stimulation in Humans: Preliminary Results - Penry - 1990 - Epilepsia - Wiley Online Library, (n.d.). https://onlinelibrary.wiley.com/doi/abs/10.1111/j.1528-1157.1990.tb05848.x (accessed January 17, 2024).

[11] Full article: A review of vagus nerve stimulation as a therapeutic intervention, (n.d.). https://www.tandfonline.com/doi/full/10.2147/JIR.S163248 (accessed January 17, 2024).

[12] Rates and Predictors of Seizure Freedom With Vagus Nerve Stimulation for Intractable Epilepsy - PMC, (n.d.). https://www.ncbi.nlm.nih.gov/pmc/articles/PMC4884552/ (accessed January 17, 2024).

[13] Prospective Long-Term Study of Vagus Nerve Stimulation for the Treatment of Refractory Seizures - DeGiorgio - 2000 - Epilepsia - Wiley Online Library, (n.d.). https://onlinelibrary.wiley.com/doi/abs/10.1111/j.1528-1157.2000.tb00325.x (accessed January 17, 2024).

[14] K. Fountas, E.Z. Kapsalaki, eds., Epilepsy Surgery and Intrinsic Brain Tumor Surgery: A Practical Atlas, Springer International Publishing, Cham, 2019. https://doi.org/10.1007/978-3-319-95918-4.

[15] Vagus nerve stimulation therapy in depression and epilepsy: therapeutic parameter settings - Labiner - 2007 - Acta Neurologica Scandinavica - Wiley Online Library, (n.d.). https://onlinelibrary.wiley.com/doi/full/10.1111/j.1600-0404.2006.00732.x?casa_token=-cyIHzThRcoAAAAA%3AYr7P3qZh3-vBnbJJPm-kIqHeHojp-Kp2ge2w_um0g_-5KM_63tH_-7ZSFRImy6zEKCul2Ltu5L2thcBHZg (accessed January 17, 2024).

[16] Vagus nerve stimulation (VNS) synchronized BOLD fMRI suggests that VNS in

depressed adults has frequency/dose dependent effects - ScienceDirect, (n.d.). https://www.sciencedirect.com/science/article/pii/S0022395602000134?casa_token=dwKu49z5QNsAAAAA:xRaUSdLFLT9gunnBkSTcTMS9kbgFS1am99FYxbc7DC4hVNYAnJwuHLVhaWQVeNzrWjqlYuc6SeR1 (accessed January 17, 2024).

[17] Vagal Stimulation Reduces the Severity of Maximal Electroshock Seizures in Intact Rats: Use of a Cuff Electrode for Stimulating and Recording - WOODBURY - 1991 - Pacing and Clinical Electrophysiology - Wiley Online Library, (n.d.). https://onlinelibrary.wiley.com/doi/abs/10.1111/j.1540-8159.1991.tb04053.x (accessed January 17, 2024).

[18] Vagus Nerve Stimulation - PMC, (n.d.). https://www.ncbi.nlm.nih.gov/pmc/articles/PMC5503741/ (accessed January 17, 2024).

[19] Alternative Paradigm of Selective Vagus Nerve Stimulation Tested on an Isolated Porcine Vagus Nerve, (n.d.). https://www.hindawi.com/journals/tswj/2014/310283/ (accessed January 17, 2024).

[20] J. Wells, C. Kao, K. Mariappan, J. Albea, E.D. Jansen, P. Konrad, A. Mahadevan-Jansen, Optical stimulation of neural tissue in vivo, Opt. Lett. 30 (2005) 504. https://doi.org/10.1364/OL.30.000504.

[21] Thompson, A.C., et al., Modeling of the temporal effects of heating during infrared neural stimulation. J Biomed Opt, 2013. 18(3): p. 035004.

[22] J. Wells, C. Kao, P. Konrad, T. Milner, J. Kim, A. Mahadevan-Jansen, E.D. Jansen, Biophysical Mechanisms of Transient Optical Stimulation of Peripheral Nerve, Biophys. J. 93 (2007) 2567–2580. https://doi.org/10.1529/biophysj.107.104786.

[23] Albert, E.S., et al., TRPV4 channels mediate the infrared laser-evoked response in sensory neurons. 2012. 107(12): p. 3227-3234.

[24] Infrared light excites cells by changing their electrical capacitance | Nature Communications, (n.d.). https://www.nature.com/articles/ncomms1742?error=cookies_not_supported&code=2312505a-7e18-4cff-be54-7ece6ab71877 (accessed January 17, 2024).

[25] Photons and neurons - ScienceDirect, (n.d.). https://www.sciencedirect.com/science/article/pii/S0378595514000409?casa_to

ken=58rkIleymvYAAAAA:aOZ7SI404HTVVWXHPhYxIGrz-OwiGGxlHYvNuOcc34wcTEYwq8k8BqKwKCz9cepX1fRzDUKcLSca (accessed January 17, 2024).

[26] J. Wells, C. Kao, K. Mariappan, J. Albea, E. D. Jansen, P. Konrad, A. Mahadevan-Jansen, *Opt. Lett.* 2005, 30, 504.

[27] J. Wells, P. Konrad, C. Kao, E. D. Jansen, A. Mahadevan-Jansen, *J. Neurosci. Methods* 2007, 163, 326.

[28] Albert, E.S., et al.,TRPV4 channels mediate the infrared laser-evoked response in sensory neurons. 2012. 107(12): p. 3227-3234.

[29] Albert, E., Bec, J.M., Chekroud, K., Travo, C., Gaboyard, S., Desmadryl, G., Bardin, F., Marc, I., Dumas, M.,Lenaers, G., Hamel, C., Muller, A. Ve Chabbert, C., "TRPV4 channels mediate the infrared laser-evoked response in sensory neurons." J. Neurophysiology, American Physiological Society, 107(12), 3227-3234 (2012)

[30] Cesare, P., Moriondo, A., Vellani, V., & McNaughton, P. A. (1999). Ion channels gated by heat. Proceedings of the National Academy of Sciences, 96(14), 7658-7663.

[31] Meyers, A. D. (1990). Laser reimbursement: Who pays for progress?. Lasers in surgery and medicine, 10(4), 396-400.

[32] Vakoc, B. J., Tearney, G. J., & Bouma, B. E., "Real-time microscopic visualization of tissue response to laser thermal therapy." Journal of Biomedical Optics, 12(2), 020501.(2007)

[33] Barton, J. K., "Dynamic changes in optical properties," In Optical-thermal response of laser-irradiated tissue (pp. 321-349). Springer, Dordrecht.(2010).

[34] High-speed optical frequency-domain imaging, (n.d.). https://opg.optica.org/oe/abstract.cfm?uri=OE-11-22-2953 (accessed January 17, 2024).

[35] Sensitivity advantage of swept source and Fourier domain optical coherence tomography, (n.d.). https://opg.optica.org/oe/abstract.cfm?uri=OE-11-18-2183 (accessed January 17, 2024).

[36] use of optical coherence tomography in neurology: a review | Brain | Oxford Academic, (n.d.). https://academic.oup.com/brain/article/145/12/4160/6691798 (accessed

January 17, 2024).

[37] M. Ibne Mokbul, Optical Coherence Tomography: Basic Concepts and Applications in Neuroscience Research, J. Med. Eng. 2017 (2017) 1–20. https://doi.org/10.1155/2017/3409327.

[38] Optical-coherence tomography of a dense tissue: statistics of attenuation and backscattering - IOPscience, (n.d.). https://iopscience.iop.org/article/10.1088/0031-9155/39/10/013/meta?casa_token=cNxVMKAdcqQAAAAA:3FAuJQ-6bvJcEvh5D1l6ch4KHYL7ZOG-_CzhlDPFoyhYxpBi97w9CFqqrv_9Ke0w33riynafipxXP91PKmevik1R7JzOVQ (accessed January 17, 2024).

[39] H. Gokkan, E. Güralp, S. Tozburun, A system using SPML laser in measuring the depth-resolved thermal change, in: M. Wojtkowski, Y. Yasuno, B.J. Vakoc (Eds.), Opt. Coherence Imaging Tech. Imaging Scatt. Media V, SPIE, Munich, Germany, 2023: p. 43. https://doi.org/10.1117/12.2672215.

[40] H. Gokkan, S. Tozburun, A customized scope head for OCT-guided laser stimulation of the vagus nerve, in: D. Levitz, A. Ozcan (Eds.), Opt. Biophotonics Low-Resour. Settings VIII, SPIE, San Francisco, United States, 2022: p. 3. https://doi.org/10.1117/12.2608721.

[41]Yetis, O., Guner, O., Akkaya, I., Guneli, E., Bagriyanik, A., & Tozburun, S (2022). Vagus nerve bundle stimulation using 1505-nm laser irradiation in an in-vivo rat model. Journal of Biophotonics, 15(1), e202100197.

[42]J. Joo, T.S. Kim, B.J. Vakoc, W. Oh, Robust and easy-to-operate stretched-pulse mode-locked wavelength-swept laser with an all-polarization-maintaining fiber cavity for 10 MHz A-line rate optical coherence tomography, Opt. Lett. (16)(2021) 3857–3860.

# 8. APPENDIX

## 8.1. Ethics Committee Approval

**İZMİR BİYOTIP VE GENOM MERKEZİ**
**GİRİŞİMSEL OLMAYAN ARAŞTIRMALAR ETİK KURULU (İBG-GOEK)**
**KARARI**

| | | | |
|---|---|---|---|
| **Toplantı Tarihi** | : 31/12/2021 | **Toplantı Günü** | : Cuma |
| **Toplantı Sayısı** | : 14 | **Toplantı Saati** | : 10:30 |

**Sayın Doç.Dr. Serhat TOZBURUN,**

**2021-045 Protokol No'lu;** sorumlusu olduğunuz "Optik Koherens Tomografi Güdümlü Lazer Sinir Stimülasyonu için Modüler Tarama Başlığı" başlıklı araştırmanın uygulanmasında etik açıdan sakınca olmadığına oy birliği ile karar verilmiştir.

Bilgilerinizi ve gereğini rica ederiz.

| | |
|---|---|
| **Prof. Dr. H. Alper BAĞRIYANIK**<br>**Başkan** | **Dr. Serap ERKEK ÖZHAN**<br>**Başkan Yardımcısı** |
| **Prof. Dr. Sedef AKGÜNGÖR**<br>**Üye** | **Prof. Dr. İnci ALACACIOĞLU**<br>**Üye** (Katılmadı) |
| **Prof. Dr. Gülgün OKTAY**<br>**Üye** | **Prof. Dr. Hilmi ORHAN**<br>**Üye** |
| **Prof. Dr. Şermin GENÇ**<br>**Üye** (Katılmadı) | **Doç. Dr. Canan Aslı YILDIRIM**<br>**Üye** |
| **Doç. Dr. Can KÜÇÜK**<br>**Üye** | **Dr. Öğr. Üyesi Yavuz OKTAY**<br>**Üye** |

## 8.2. Curriculum Vitae

## ÖZGEÇMİŞ

| | |
|---|---|
| **ADI SOYADI** | HANIFE GÖKKAN |
| **TC KIMLIK NO / PASAPORT NO** | 1 |
| **DOĞUM YILI** | 1997 |
| **YAZIŞMA ADRESI** | 35340, İnciraltım Mahallesi, Balçova,İzmir |
| **TELEFON** | 552 |
| **E-POSTA** | h |

### EĞİTİM BİLGİLERİ

| Ülke | Üniversite | Fakülte/Enstitü | Öğrenim Alanı | Derece | Mezuniyet Yılı |
|---|---|---|---|---|---|
| TR | Dokuz Eylül Üniversitesi | İzmir Uluslararası Biyotıp ve Genom Enstitüsü | Biyotıp ve Sağlık Teknolojileri | Yüksek Lisans | 2024 |
| TR | Pamukkale Üniversitesi | Teknoloji Fakültesi | Biyomedikal Mühendisliği | Lisans | 2020 |

### Uzmanlık Alanları

| Uzmanlık Alanları |
|---|
| Laser nerve stimulation, swept-source optical coherence tomography, optical probe, M-mode imaging. |

## Publications

1. **Gokkan H**, Guralp E, Tozburun S. "A system using SPML laser in measuring the depth-resolved thermal change" European Conferences on Biomedical Optics (ECBO) – Munich,GERMANY (Oral Presentation, 26-29 June 2023)
2. **Gokkan H** and Tozburun S. "A customized scope head for OCT-guided laser stimulation of the vagus nerve" SPIE Photonics West BIOS- San Francisco, USA (Oral Presentation,22-27 Jan 2022